

# Argonne National Laboratory

## DEVELOPMENT OF HIGH-ENERGY BATTERIES FOR ELECTRIC VEHICLES

Progress Report for  
February 1969 through June 1970

by

E. J. Cairns, M. L. Kyle, V. A. Maroni,  
H. Shimotake, R. K. Steunenberg,  
and A. D. Tevebaugh

The facilities of Argonne National Laboratory are owned by the United States Government. Under the terms of a contract (W-31-109-Eng-38) between the U. S. Atomic Energy Commission, Argonne Universities Association and The University of Chicago, the University employs the staff and operates the Laboratory in accordance with policies and programs formulated, approved and reviewed by the Association.

#### MEMBERS OF ARGONNE UNIVERSITIES ASSOCIATION

The University of Arizona	Kansas State University	The Ohio State University
Carnegie-Mellon University	The University of Kansas	Ohio University
Case Western Reserve University	Loyola University	The Pennsylvania State University
The University of Chicago	Marquette University	Purdue University
University of Cincinnati	Michigan State University	Saint Louis University
Illinois Institute of Technology	The University of Michigan	Southern Illinois University
University of Illinois	University of Minnesota	The University of Texas at Austin
Indiana University	University of Missouri	Washington University
Iowa State University	Northwestern University	Wayne State University
The University of Iowa	University of Notre Dame	The University of Wisconsin

#### NOTICE

This report was prepared as an account of work sponsored by the United States Government. Neither the United States nor the United States Atomic Energy Commission, nor any of their employees, nor any of their contractors, subcontractors, or their employees, makes any warranty, express or implied, or assumes any legal liability or responsibility for the accuracy, completeness or usefulness of any information, apparatus, product or process disclosed, or represents that its use would not infringe privately-owned rights.

Printed in the United States of America  
Available from  
National Technical Information Service  
U.S. Department of Commerce  
Springfield, Virginia 22151  
Price: Printed Copy \$3.00; Microfiche \$0.65

ARGONNE NATIONAL LABORATORY  
9700 South Cass Avenue  
Argonne, Illinois 60439

DEVELOPMENT OF HIGH-ENERGY BATTERIES  
FOR ELECTRIC VEHICLES

Progress Report for  
February 1969 through June 1970

by

E. J. Cairns, M. L. Kyle, V. A. Maroni,  
H. Shimotake, R. K. Steunenberg,  
and A. D. Tevebaugh

Chemical Engineering Division

July 1970

## FOREWORD

This is the first technical progress report of a research and development program conducted by the Chemical Engineering Division of Argonne National Laboratory under an agreement between the United States Atomic Energy Commission and the Environmental Protection Agency, Air Pollution Control Office, Division of Motor Vehicle Research and Development. The period covered by this report is February 1, 1969 through June 30, 1970.

The long-term goal of this program is to develop the technology for the construction and testing of a 20-kW average power lithium/sulfur battery suitable for powering an electric family automobile. The immediate goals are the development and scale-up of single lithium/sulfur cells, followed by the construction and testing of small (1-2 kW) batteries.

Overall program management is the responsibility of Dr. R. C. Vogel, Division Director, and Dr. A. D. Tevebaugh, Associate Division Director. Technical direction is provided by Dr. E. J. Cairns, Section Head, and Dr. R. K. Steunenberg, Group Leader.

## TABLE OF CONTENTS

	<u>Page</u>
Abstract	1
Summary	1
I. Introduction	3
II. Experimental Procedures	6
A. Investigations of Small-Scale Lithium/Sulfur and Lithium/P <sub>x</sub> S <sub>y</sub> Cells	6
B. Corrosion Tests	9
III. Results and Discussion	13
A. Investigation of Small-Scale Lithium/Sulfur Cells	13
1. Liquid-Electrolyte Cells	13
a. Short-Term Voltage-Current Density Characteristics	15
b. The Effect of Temperature on Lithium/Sulfur Cell Performance	15
c. The Effect of Cathode Current-Collector Porosity and Pore Size on Lithium/Sulfur Cell Performance	17
d. Relationship Between Current Density and Capacity Density	22
e. Effect of Current-Collector Geometry on Lithium/Sulfur Cell Performance	22
f. Cells with Sulfur-Phosphorus Compounds as Cathode Materials	28
g. Effect of Cell Geometry on Lithium/Sulfur Cell Performance	28
2. Paste-Electrolyte Cells	35
a. Electrical Performance	35
b. Filler Stability	37
B. Results of Corrosion Tests	39
1. Rigid Electrical Insulators	39
2. Pliable Electrical Insulators	41

Table of Contents (Continued)

Page

3. Electrically Conducting Materials	43
a. Results of 100- to 300-Hour Screening Tests	43
b. Results of 600-Hour Tests	46
IV. Conclusions	50
Acknowledgments	51
References	52

LIST OF FIGURES

<u>Figure No.</u>	<u>Title</u>	<u>Page</u>
1	Lithium/Sulfur Cell with Liquid Electrolyte	7
2	Experimental Lithium/Sulfur Cell with Paste Electrolyte	10
3	Tube Furnace for Corrosion Agitator Experiments	12
4	Reactions in a Lithium/Sulfur Cell	14
5	Voltage-Current Density Characteristics of Lithium/Sulfur Cells	16
6	Effect of Temperature on Lithium/Sulfur Cell Performance	19
7	Experimental Lithium/Sulfur Cell	20
8	Relationship Between the Porosity of the Cathode Current Collector and the Capacity Density of Lithium/Sulfur Cells	23
9	Capacity Density-Current Density Relationship for Various Cathode Current Collectors	24
10	Effect of Cathode Thickness on the Capacity Density-Current Density Characteristics of Lithium/Sulfur Cells	27
11	Comparison of Voltage-Capacity Density Data for Lithium/Sulfur, Lithium/P <sub>4</sub> S <sub>10</sub> and Lithium/P <sub>4</sub> S <sub>3</sub> Cells	30
12	Laminated-Cathode Lithium/Sulfur Cell	32
13	Voltage-Current Density Data for Lithium/Sulfur Cell with Laminated Cathode	33
14	Voltage-Capacity Density Data for Lithium/Sulfur Cell with Laminated Cathode	34
15	Voltage-Capacity Density Data for Lithium/Sulfur Cell with Paste Electrolyte	36
16	Corrosion of Electrical Insulators by Molten Lithium	42
17	Corrosion of Metals by Molten Lithium-Sulfur Mixtures	48

LIST OF TABLES

<u>Table No.</u>	<u>Title</u>	<u>Page</u>
I	Effect of Temperature on Lithium/Sulfur Cell Performance	18
II	Characteristics of Cathode Structures and Cell Performance	21
III	Effect of Cathode Current Collector Structure on Lithium/Sulfur Cell Performance	26
IV	Comparison of Lithium/Sulfur, Lithium/P <sub>4</sub> S <sub>10</sub> and Lithium/P <sub>4</sub> S <sub>3</sub> Cells	29
V	Corrosion of Electrical Insulators by Molten Lithium-Sulfur Mixtures	40
VI	Corrosion of Metals by Molten Lithium-Sulfur Mixtures: Screening Tests	44
VII	Chemical Compositions of Metals Tested in Molten Lithium-Sulfur Mixtures	45
VIII	Corrosion of Metals by Molten Lithium-Sulfur Mixtures: 620-Hr Tests	47

# DEVELOPMENT OF HIGH-ENERGY BATTERIES FOR ELECTRIC VEHICLES

by

E. J. Cairns, M. L. Kyle, V. A. Maroni,  
H. Shimotake, R. K. Steunenbergh,  
and A. D. Tevebaugh

## ABSTRACT

The applicability of lithium/chalcogen cells to secondary batteries for vehicular propulsion is being investigated. During this period, cathode materials containing sulfur,  $P_4S_{10}$ , and  $P_4S_3$  were tested in cells operated at 325-400°C. Liquid-electrolyte lithium/sulfur cells have exhibited capacity densities from 0.1-0.2 A-hr/cm<sup>2</sup> at a current density of 0.5 A/cm<sup>2</sup>. Sulfur utilization has usually been less than 35%. Cathode current-collector structure was found to have a significant effect on cell performance. Improved capacity density, near 0.5 A-hr/cm<sup>2</sup> at a current density of 0.5 A/cm<sup>2</sup>, was achieved by means of a laminated cathode structure. Potential construction materials for lithium/sulfur cells were subjected to 600-hr corrosion tests at 375°C. Molybdenum, chromium, and niobium showed corrosion rates sufficiently low for use in cells of anticipated lifetimes greater than 1000 hr.

## SUMMARY

This report covers work performed between February 1969 and June 1970 under an agreement between the National Air Pollution Control Administration of CPE, Public Health Service, U. S. Department of Health, Education and Welfare and the United States Atomic Energy Commission. Under this agreement, the Chemical Engineering Division of Argonne National Laboratory is investigating the performance characteristics of lithium/chalcogen cells to evaluate their applicability as secondary (electrically rechargeable) batteries for vehicular propulsion.

During this period, the experimental investigations were directed toward the Li/LiF-LiCl-LiI/Li in S, Li/LiBr-RbBr/Li in S, Li/LiBr-RbBr/Li in  $P_4S_{10}$ , and Li/LiBr-RbBr/Li in  $P_4S_3$  cells at temperatures from 325-400°C. Small-scale (~ 1-cm<sup>2</sup> electrode area) liquid and paste electrolyte cells were operated to determine those conditions under which the cells will deliver current densities of 0.3 to 1 A/cm<sup>2</sup> for a large fraction of their capacity densities. Cells of this type require capacity densities of about 0.4 A-hr/cm<sup>2</sup> at current densities of 0.3 to 1.0 A/cm<sup>2</sup> to achieve the performance required by electric vehicles.

Liquid-electrolyte lithium/sulfur cells have, in general, exhibited capacity densities from 0.1 to 0.2 A-hr/cm<sup>2</sup> at a current density of

0.5 A/cm<sup>2</sup>. Sulfur utilization has usually been under 35%. Cell performance is believed to be limited by two main factors, (1) the low diffusion rate of the cell reaction products away from the sulfur-electrolyte interface, and (2) the low electronic conductivity of sulfur. Studies of variables which promise to increase cell performance were conducted. The effects of cell operating temperature, additives to reduce the viscosity of sulfur, cathode current-collector structure and design, and alternative cathode materials have been measured. Cathode current-collector structure was found to have a significant effect on cell performance.

A modification of the cell design to provide an increased sulfur-electrolyte interfacial area by means of a laminated cathode structure resulted in increased cell performance. This design produced capacity densities near 0.5 A-hr/cm<sup>2</sup> at a current density of 0.5 A/cm<sup>2</sup>. With this type of design, however, this same performance must be achievable in about one-third the experimental cathode volume to satisfy the performance requirements of electric vehicles.

Corrosion tests of potential materials of construction for lithium/sulfur cells were made with a variety of materials including some representative austenitic and ferritic stainless steels, manganese-chromium stainless steels, nickel-base alloys, and pure elements. Of the materials subjected to 600-hr corrosion tests at 375°C, only molybdenum, chromium, and niobium showed corrosion rates sufficiently low for use in cells of anticipated lifetimes greater than 1000 hr.

## I. INTRODUCTION

Over 60 percent of the total air pollution in the United States and up to 90 percent of that in the large cities is attributed to motor vehicles. (1,2) Although improvements in engine design, fuels, and emission control devices such as catalytic combustors and afterburners show promise of achieving a significant reduction in the amount of emission per vehicle, these approaches appear to be only temporary expedients because of the anticipated increase in the number of vehicles. (3-5) The use of battery-powered electric vehicles is a possible means of bringing about a substantial decrease in the amount of air pollution. The required electrical energy would then be generated by efficient fossil-fueled power stations or by nuclear facilities. The main problem that must be overcome in achieving practical electric vehicles for general use is the present lack of low-cost secondary batteries that have sufficient energy-storage capacity per unit weight.

Recent studies (1,6,7) have shown that it will be necessary to make a major improvement in the specific energy (W-hr/kg) of batteries without sacrificing the peak specific power (W/kg) before electric passenger vehicles will become technically attractive. Depending on the design and materials of an electric passenger vehicle, a range approaching 200 miles and an acceptable acceleration capability would require a battery having a specific energy of at least 200 W-hr/kg and a peak specific power of at least 200 W/kg. To be economically feasible (*i.e.*, competitive with current internal combustion engines) the battery should cost no more than about \$2/kg (or about \$10/kW-hr). (6,7) The requirements for a city taxi, bus, or delivery vehicle are somewhat less severe (6-9) because of less stringent requirements for both acceleration and range.

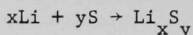
The specific energy requirement of 200 W-hr/kg excludes all conventional secondary batteries from further consideration as a power source for general use in electric vehicles because none of them is likely to achieve this energy-storage capability. (10,11) Among the aqueous-electrolyte electrochemical cells now under development, only the zinc/air cell shows some promise of achieving 200 W-hr/kg. (12-14) Several high-specific-energy cells with organic-solvent electrolytes (15) are under development at various laboratories, but neither these nor the zinc/air cell can provide the high specific power (above 200 W/kg) that is needed for the acceleration required in present traffic-flow patterns.

The only class of cells currently under investigation that shows promise for development into high-specific-energy, high-specific-power secondary batteries consists of cells that operate at elevated temperatures. (6) These cells employ lithium or sodium anodes (of low electronegativity, low equivalent weight, and high exchange-current density), molten-salt or cation-conducting solid electrolytes, and

cathode materials of groups VI or VII of the periodic chart<sup>(11)</sup> (the chalcogens and halogens have high electronegativity, moderate-to-low equivalent weights and high exchange-current densities). Cells of this type have already been built and tested in various laboratories. These include the lithium/chlorine cell,<sup>(16-18)</sup> the sodium/sulfur cell<sup>(19)</sup> the lithium/tellurium cell,<sup>(20,21)</sup> the lithium/selenium cell<sup>(22,23)</sup> and the lithium/sulfur cell.<sup>(10,24)</sup>

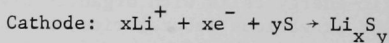
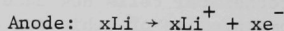
A modest experimental program has been carried out at Argonne National Laboratory on cells of the types Li/LiX/S and Li/LiX/P<sub>x</sub>S<sub>y</sub>, which show promise of meeting the requirements of low cost, high specific energy and high specific power for electric vehicle batteries. In these cell representations, LiX is a low-melting salt containing lithium halide which is used either as a liquid electrolyte or as a paste with an inert filler material. The two electrolytes used during the experimental program are the eutectic salts 59 mole % LiBr-41 mole % RbBr (melting point ~ 278°C) and 11.7 mole % LiF-29.1 mole % LiCl-59.2 mole % LiI (melting point ~ 341°C). The phosphorus-sulfur compounds investigated as cathode materials were P<sub>4</sub>S<sub>3</sub> and P<sub>4</sub>S<sub>10</sub>.

The overall reaction that takes place upon discharge of a lithium/sulfur cell can be written as



where the product may be Li<sub>2</sub>S, or some other compound of lithium and sulfur, depending upon the amounts of lithium and sulfur in the cell and the amount of electrical charge which has been withdrawn from the cell (the extent of the cell reaction). Under most operating conditions, the product of the cell reaction is soluble in the excess sulfur at the cathode; however, the product Li<sub>2</sub>S is allowed to precipitate during the later stages of discharge. The product redissolves on recharging.

The electrode reactions corresponding to the overall cell reaction given above are



At the anode, lithium metal is oxidized to lithium cations which migrate through the fused lithium halide electrolyte, and electrons which pass through the electrical circuit, doing work as they go. At the cathode, lithium cations from the electrolyte are neutralized by electrons from the electrical circuit, forming lithium atoms which react immediately to form the lithium sulfide Li<sub>x</sub>S<sub>y</sub>, which is soluble in excess sulfur. As the cell is discharged further, Li<sub>x</sub>S<sub>y</sub> accumulates in the cathode, finally exceeds the solubility limit, and precipitates. At this point, the cell voltage becomes constant, and solid Li<sub>x</sub>S<sub>y</sub> accumulates until the

cathode is completely solid. Normally, the cell is not discharged to the solidification point. The reverse of these processes occurs on recharging the cell.

The cathode from a discharged lithium/sulfur cell was examined to identify the reaction products. X-ray diffraction analysis indicated the presence of nearly pure  $\text{Li}_2\text{S}$  in some locations of the cell, and  $\text{Li}_2\text{S}$  is believed to be the end product of the reaction.

The work on this program has consisted mainly of electrical performance tests of small experimental cells, corrosion tests of various materials, and preliminary design studies of lithium/sulfur batteries for electric vehicles. This report summarizes the results of this effort since February 1969.

## II. EXPERIMENTAL PROCEDURES

### A. Investigation of Small-Scale Lithium/Sulfur and Lithium/P<sub>x</sub>S<sub>y</sub> Cells

#### 1. Liquid-Electrolyte Cells

The operation of lithium/sulfur and lithium/P<sub>x</sub>S<sub>y</sub> cells was carried out in a resistance-heated furnace well attached to the floor of a glovebox containing a helium atmosphere of high purity.<sup>(25)</sup> The helium purification unit maintained an atmosphere containing < 5 ppm each of water, oxygen and nitrogen. Low water and oxygen levels are required to prevent contamination of the lithium electrode and electrolyte.

Several different cell configurations were used during the series of experiments. Figure 1 shows a liquid-electrolyte cell typical of those used in the experimental investigations. The anode compartment is a small stainless steel cup containing stainless steel Feltmetal.\* The Feltmetal was washed with xylene prior to use to remove any residual oil and grease that may have been present from manufacture and handling. The anode cup containing the stainless steel Feltmetal mesh was heated to 600°C and loaded with an appropriate amount of lithium. At 600°C lithium readily wets the stainless steel. Good wetting of the Feltmetal by lithium is necessary because lithium is less dense than the molten salt electrolyte and would tend to float to the surface in the particular cell if the stainless steel Feltmetal were not well wetted.

The cathode compartment of the cell is a small niobium housing containing a sulfur-impregnated porous current-collector structure. This housing is tight fitting and gasketed at the upper end to inhibit sulfur vaporization losses from the cell during the course of an experiment.

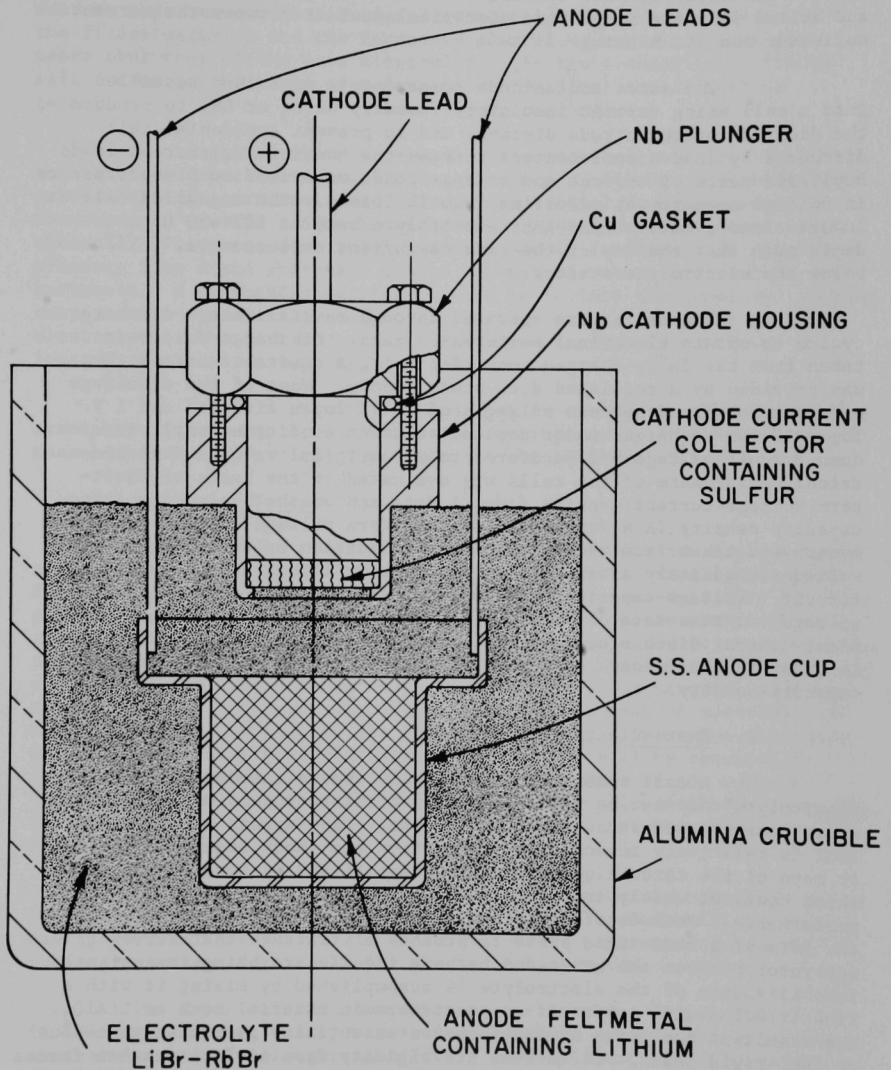
The cathode current collector is required because sulfur is a very poor electronic conductor ( $3.3 \times 10^{-8} \text{ ohm}^{-1} \text{ cm}^{-1}$  at 375°C). An electronically conducting material is required to distribute electrons to the sites of electrochemical reaction which are located at the cathode-electrolyte interface. This current collector must not interfere unduly with the transport of lithium-sulfur reaction products away from the cathode-electrolyte interface, or the transport of sulfur to it. Because of the conflicting requirements for current collection and mass transport, the cathode current-collector design has a strong influence on cell performance, and its design is one of the variables under investigation.

The cathode current collectors were also degreased with xylene before use and were filled with molten sulfur by immersion in a molten sulfur bath at  $\sim 150^\circ\text{C}$  under vacuum to remove entrapped gases.

---

\* Trademark of Huyck Metals Co.

Figure 1. Lithium/Sulfur Cell with Liquid Electrolyte



At about 150°C sulfur has a minimum viscosity which permits the small pores of the current collector to be readily filled with sulfur. The sulfur-containing cathode current collector was placed in its housing and bolted in place to provide electrical contact between the current collector and its housing.

The anode and cathode compartments were then assembled into a cell using ceramic insulators (usually  $\text{Al}_2\text{O}_3$  or BN) to produce the desired interelectrode distance and to prevent accidental cell discharge by inadvertent contact between the housings or current leads. Duplicate pairs of current and voltage leads were used to prevent errors in voltage measurement resulting from IR losses. The assembled cell was lowered into a molten LiBr-RbBr electrolyte bath at 325-400°C to a depth such that the top of the cathode current collector was  $\sim 1/2$  cm below the electrolyte surface.

The cells were operated through several charge-discharge cycles to obtain electrical performance data. Discharge data were taken from the fully-charged condition using a constant current that was provided by a regulated d.c. power supply. Most of the discharge data were obtained between voltages of 2.3 V (open circuit) and 1 V. The cell was recharged under constant current conditions until the open-circuit voltage had recovered to its original value. The electrical performance of the cells was evaluated on the basis of short-term voltage-current density ( $\text{A}/\text{cm}^2$ ) data and on the basis of voltage-capacity density ( $\text{A}\cdot\text{hr}/\text{cm}^2$ ) data. Short-term voltage-current measurements were taken from the fully-charged condition by recording the cell voltage immediately after closing the switch in the current-carrying circuit. Voltage-capacity density data were calculated from the cell voltage vs. time data obtained under constant-current discharge. Constant-current discharges were performed at various current densities in order to obtain data on the relationship between current density and capacity density.

## 2. Paste-Electrolyte Cells

A cell combining three liquid phases (anode, cathode and electrolyte) may not be practical for vehicular propulsion applications where motion could cause short-circuiting. Development of a battery that is relatively insensitive to position and shock requires that one or more of the three liquid phases be immobilized by some simple method which does not unduly increase the weight of the cell or decrease its performance. Methods of immobilizing the molten-salt electrolyte in the form of a semi-rigid paste to produce a structure that serves as a separator between the anode and cathode liquids are being investigated. Immobilization of the electrolyte is accomplished by mixing it with a fine ( $< 0.1 \mu$  dia) powder of an inert ceramic material such as  $\text{LiAlO}_2$ . The resultant two-phase mixture behaves essentially as a highly viscous or semi-rigid paste. It derives its rigidity from surface tension forces acting upon the fine filler particles, but still retains enough plasticity to distort slightly under stress at temperatures above the melting

point of the electrolyte.

In the preparation of the paste electrolyte, a compromise must be made between the increased strength and rigidity imparted by the filler material and the increased electrical resistivity of the paste over that of the pure electrolyte. At the present time, filler:salt ratios in the range of 4:6 to 6:4 (by weight) are of most interest.

Figure 2 shows a typical paste-electrolyte cell. The anode and cathode compartments are similar to those of liquid-electrolyte cells except that they are contained in more substantial housings, which are necessary to provide alignment and prevent liquid or vapor losses from the cell. The paste electrolyte molding powder is formed<sup>(23)</sup> under high pressure into disks which are placed between the anode and cathode compartments. A BN insulating ring is used to isolate the anode and cathode compartments electrically and to provide radial restraint for the paste electrolyte. The entire assembly is clamped together to minimize the loss of reactants during cell operation.

The cell assembly is operated in a resistance-heated, helium-atmosphere furnace well, and electrical performance characteristics are measured in a manner similar to that for the liquid-electrolyte cell.

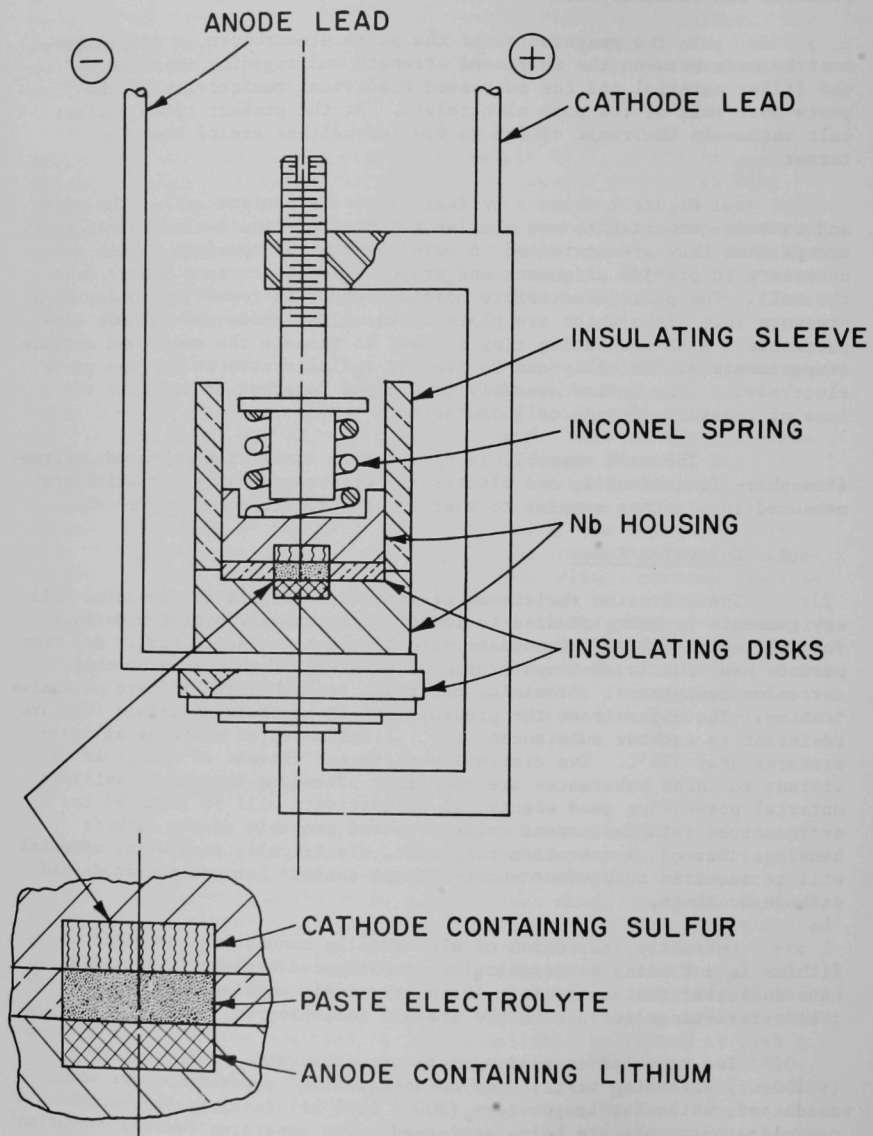
#### B. Corrosion Tests

The corrosion resistance of various materials to simulated cell environments is being studied to identify potentially useful materials for cell applications. Candidate materials are tested initially for time periods near 100 hr at temperatures of about 375°C to determine their corrosion resistance. Promising materials are subjected to more extensive testing. The emphasis at the present time is on those materials that are resistant to cathode substances, *i.e.*, lithium-sulfur mixtures at temperatures near 375°C. Two distinctly different classes of materials resistant to these substances are required: First, a corrosion-resistant material possessing good electrical conductivity will be required to serve as the cathode current collector, and probably as the cathode housing. Second, a corrosion-resistant, electrically insulating material will be required to prevent short-circuit contact between the anode and cathode housings.

Currently, corrosion of electrically conducting materials by lithium is not being systematically investigated because cell studies have indicated that austenitic stainless steels possess adequate corrosion resistance for use in the present cell program.

Two types of corrosion tests are performed. For short-term ( $\sim$  100-hr) screening tests, "corrosion-agitator" experiments are being conducted, while for longer-term (200 - 1000 hr) testing, isothermal capsule experiments are being performed. The apparatus for the corrosion

Figure 2. Experimental Lithium/Sulfur Cell with Paste Electrolyte



agitator tests is shown in Figure 3. In these tests, the corrosion specimen (about 1.25 x 1.88 x 0.16 cm) is exposed to the lithium-sulfur mixture (about 50 cc) as a slowly rotating paddle. This method of exposure was chosen because many materials are protected from corrosion by formation of a surface film. Such a film may be protective under static conditions, but may be removed under dynamic conditions. The slow rotation of the paddle is intended to approximate roughly the mass-transfer conditions that might be experienced in some battery applications.

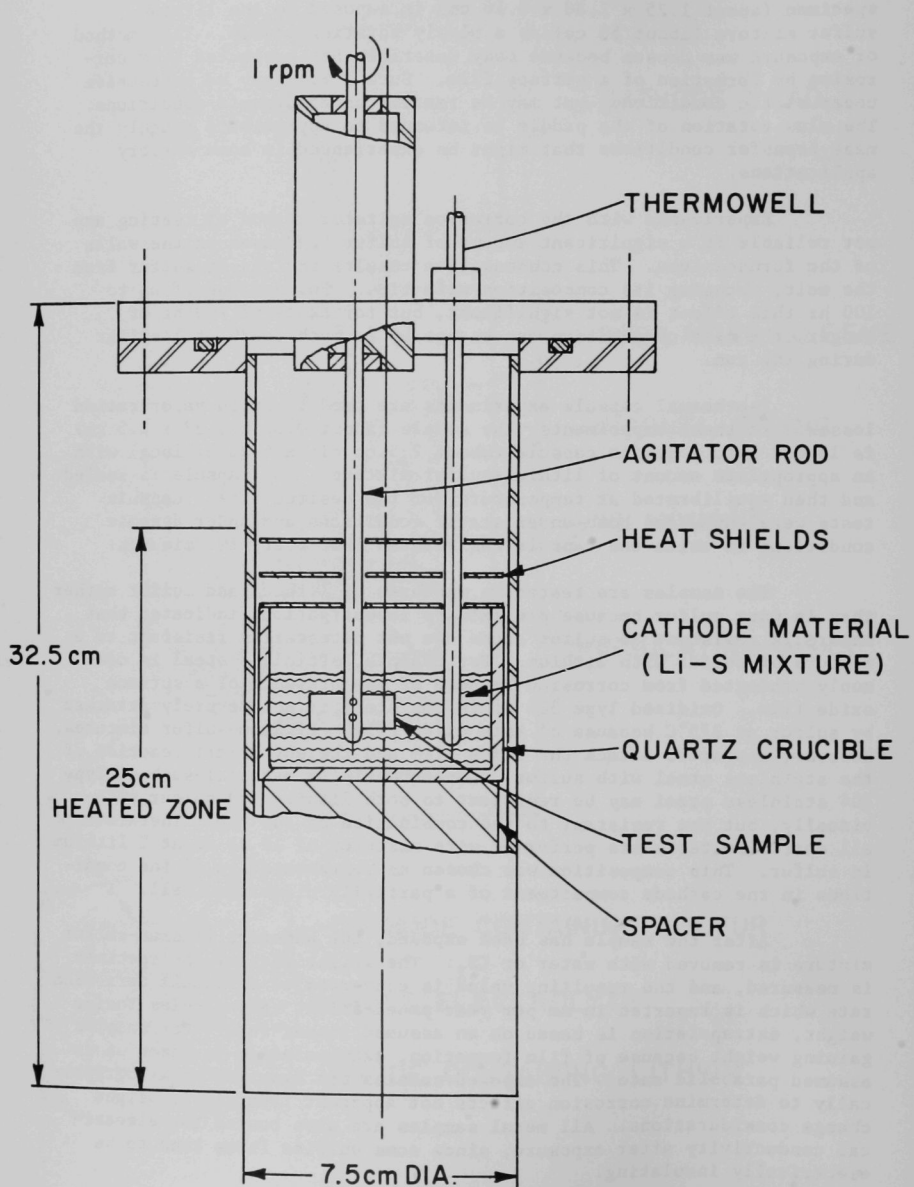
Experiments with the corrosion agitator method of testing are not reliable if a significant amount of sulfur condenses on the walls of the furnace tube. This condensation results in loss of sulfur from the melt, changing its composition with time. For periods of up to 100 hr this effect is not significant, but for tests of 200 hr or longer, the melt composition can change by as much as 20 at.% sulfur during the run.

Isothermal capsule experiments are used to avoid vaporization losses. In these experiments, the sample (about 0.32 x 0.32 x 2.5 cm) is loaded into a quartz capsule (about 2.5 cm dia x 6.25 cm long) with an appropriate amount of lithium-sulfur mixture. The capsule is sealed and then equilibrated at temperature for the desired time. Capsule tests were conducted both under static conditions and under dynamic conditions in which the capsule was rotated 180° every two minutes.

The samples are tested in mixtures of lithium and sulfur rather than in pure sulfur because preliminary investigations indicated that materials resistant to sulfur alone are not necessarily resistant to a mixture of sulfur with lithium. For example, stainless steel is commonly protected from corrosion because of the presence of a surface oxide film. Oxidized Type 304 stainless steel is not severely attacked by sulfur at 375°C because of this oxide film. Lithium-sulfur mixtures, however, appear to attack the oxide film and thereby permit reaction of the stainless steel with sulfur. Consequently, a material such as Type 304 stainless steel may be resistant to both lithium and sulfur individually, but not resistant to the combination of the two. Therefore, all corrosion tests are performed with mixtures of 10 to 20 at.% lithium in sulfur. This composition was chosen as representative of the conditions in the cathode compartment of a partially discharged cell.

After the sample has been exposed, any adhering lithium-sulfur mixture is removed with water or  $CS_2$ . The weight loss of the specimen is measured, and the resulting value is converted to an annual corrosion rate which is reported in mm per year penetration. For samples losing weight, extrapolation is based on an assumed linear rate. For samples gaining weight because of film formation, extrapolation is based on an assumed parabolic rate. The exposed samples are examined metallographically to determine corrosion effects not apparent from simple weight change considerations. All metal samples are also tested for electrical conductivity after exposure, since some sulfide films tend to be electrically insulating.

Figure 3. Tube Furnace for Corrosion Agitator Experiments



### III. RESULTS AND DISCUSSION

#### A. Investigation of Small-Scale Lithium/Sulfur Cells

##### 1. Liquid-Electrolyte Cells

(M. L. Kyle, H. Shimotake, F. J. Martino, J. C. Cassulo)

Liquid-electrolyte cells of the types Li/LiBr-RbBr/Li in S and Li/LiBr-RbBr/Li in P<sub>2</sub>S<sub>5</sub> were investigated at operating temperatures from 325 to 400°C. The objective of these investigations was to determine those conditions under which the cells achieve a high capacity density (0.4 A-hr/cm<sup>2</sup> or greater) at current densities compatible with the requirements of an electric vehicle (0.3 A/cm<sup>2</sup> or greater).

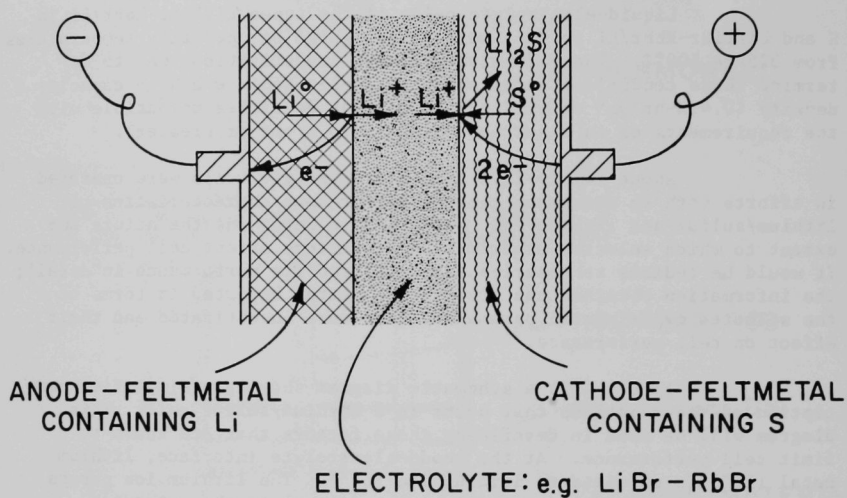
About twenty-five liquid-electrolyte cells were operated in efforts both to determine typical performance characteristics of lithium/sulfur and lithium/P<sub>2</sub>S<sub>5</sub> cells and to determine the nature and extent to which selected experimental parameters affect cell performance. It would be tedious to describe each cell and its performance in detail; the information obtained can probably be better reported in terms of the selected experimental parameters that were investigated and their effect on cell performance.

Figure 4 is a schematic diagram showing a simplified conception of the reactions that occur in a lithium/sulfur cell. This diagram will be used in describing those factors that are known to limit cell performance. At the anode-electrolyte interface, lithium metal (Li<sup>0</sup>) is oxidized to lithium ion (Li<sup>+</sup>). The lithium ion passes through the electrolyte (a good ionic conductor) to the cathode-electrolyte interface where two lithium ions, a sulfur atom (S<sup>0</sup>) and two electrons (e<sup>-</sup>) combine to form the cell reaction product, Li<sub>2</sub>S. The Li<sub>2</sub>S cell product must diffuse away from the cathode/electrolyte interface in order to allow additional sulfur to contact the electrolyte. Slow diffusion of the Li<sub>2</sub>S limits the rate of the cathode reaction. The high viscosity of sulfur (~ 1000 cp)<sup>(26)</sup> and its tendency to form polymer chains inhibit the diffusion of Li<sub>2</sub>S away from the interface.

Various means for increasing the rate of the overall cathode reaction have been investigated, including (a) increasing the operating temperature to decrease the viscosity of sulfur and thus increase the rate at which Li<sub>2</sub>S diffuses away from the cathode-electrolyte interface, (b) adding various materials to the sulfur in order to decrease its viscosity (chain-breakers and chain stoppers), (c) modifying the cathode geometry to increase the area of the cathode-electrolyte interface per unit of projected cathode area.

The diffusion of the cell reaction product away from the interface causes the cell capacity density to be related to the current density. At a high rate of discharge, the reaction products are formed

Figure 4. Reactions in a Lithium/Sulfur Cell



#### CELL REACTIONS

CELL:  $\text{Li}/\text{Li}^+(\text{ELECTROLYTE})/\text{S} (+\text{Li})$

ANODE:  $\text{Li}^\circ \rightarrow \text{Li}^+ + \text{e}^-$

CATHODE:  $2\text{Li}^+ + 2\text{e}^- + \text{S}^\circ \rightarrow \text{Li}_2\text{S}$

OVERALL:  $2\text{Li}^\circ + \text{S}^\circ \rightarrow \text{Li}_2\text{S}$

at the interface more rapidly than they can diffuse away. The buildup of products at the interface increases the diffusion overvoltage and the internal resistance of the cell, causing the cell voltage to decrease below some lower limit (1 volt) before all of the sulfur is reacted.

The low electronic conductivity of sulfur interferes with the cathode reaction because it limits the rate at which electrons are transported to the sulfur-electrolyte interface, and limits the extent to which the interface is useful. The cathode current collector is a porous metal structure which provides a path for electrons to reach the interface. The current-collector geometry, therefore, has somewhat conflicting requirements. A small-pore-size body provides more and shorter electron paths through the sulfur. If, however, these pores are too small, they will inhibit the  $\text{Li}_2\text{S}$  diffusion rate and lower the cell performance. Consequently, the porosity (percent porosity + percent of theoretical density = 100%) and average pore diameter (the actual pore diameters usually range from about one-half to twice the average reported) of the cathode current collector are important variables affecting cell performance.

The electrolyte resistance to lithium ion flow is the main variable affecting the short-term voltage-current density characteristics of the cell. This resistance is a function primarily of electrolyte composition, electrode area, and interelectrode distance ( $R = \rho \frac{l}{A}$ ). Despite the fact that the electrolyte resistance varies slightly with temperature and that the overall short-term cell resistance is also affected by anode and cathode contact resistances, the magnitudes of these effects are small when compared to the electrolyte contribution in short-term data.

#### a. Short-Term Voltage-Current Density Characteristics

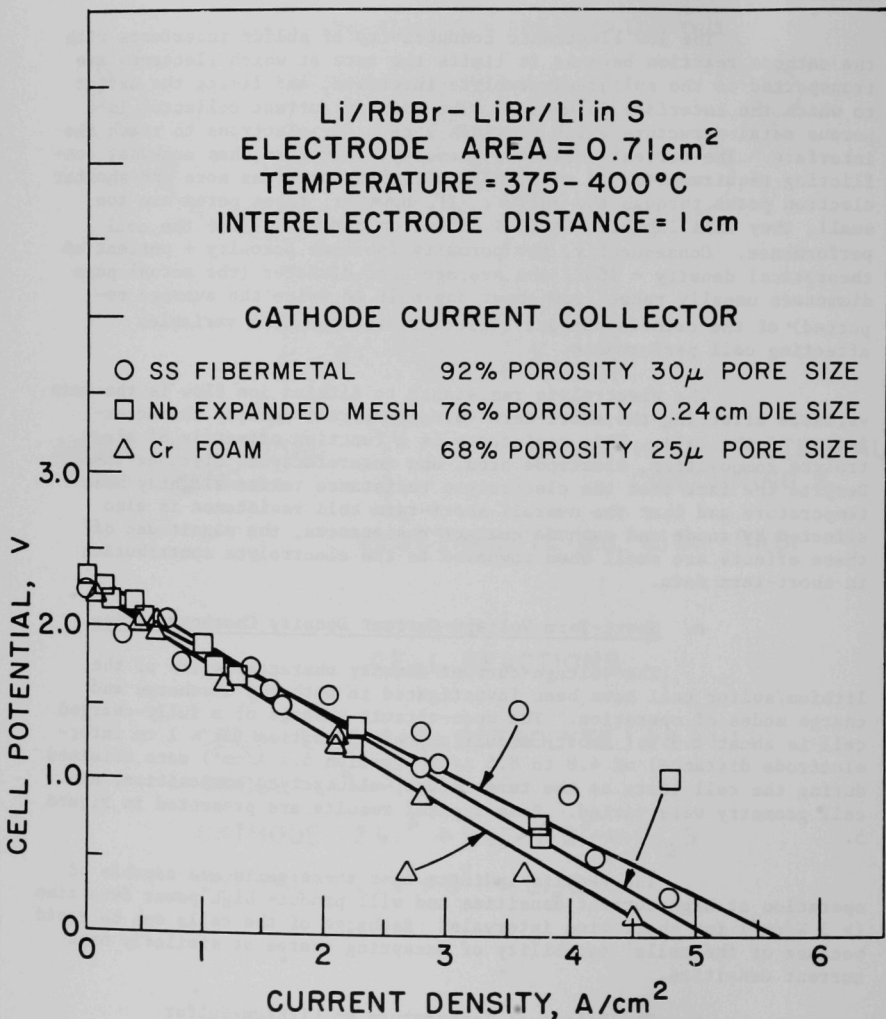
The voltage-current density characteristics of the lithium/sulfur cell have been investigated in both the discharge and charge modes of operation. The open-circuit voltage of a fully-charged cell is about 2.3 V. Short-circuit current densities (at  $\sim 1$  cm interelectrode distance) of 4.8 to 8.5  $\text{A}/\text{cm}^2$  (median 6.4  $\text{A}/\text{cm}^2$ ) were obtained during the cell tests as the temperature, electrolyte composition, and cell geometry were varied. Some typical results are presented in Figure 5.

The results indicate that these cells are capable of operation at high current densities and will produce high power densities ( $> 3 \text{ W}/\text{cm}^2$ ) for short time intervals. Recharge of the cells can be rapid because of the cells' capability of accepting charge at similarly high current densities.

#### b. The Effect of Temperature on Lithium/Sulfur Cell Performance

An increase in temperature increases the diffusion rate

Figure 5. Voltage-Current Density Characteristics of Lithium/Sulfur Cells



of the reaction product in the cathode, and thereby increases cell performance. The effect can be seen in Table I by comparing the performance of Cells 21 and 22 at a current density of about  $1 \text{ A/cm}^2$ . At a temperature of  $364^\circ\text{C}$ , Cell 21 had a capacity density of  $0.022 \text{ A-hr/cm}^2$ , compared to  $0.052 \text{ A-hr/cm}^2$  at  $385^\circ\text{C}$  for Cell 22. In all other respects, these cells were similar. The temperature of Cell 25, which had a molybdenum foam cathode current collector, was varied during its operation. At current densities of both  $0.33$  and  $1.03 \text{ A/cm}^2$ , a temperature increase of about  $50^\circ\text{C}$  ( $350^\circ\text{C}$  to  $400^\circ\text{C}$ ) nearly doubled the measured capacity density of the cell. These data, shown in Figure 6, demonstrate the strong temperature dependence of capacity density. Efforts to reduce the operating temperature of lithium/sulfur cells to around  $300^\circ\text{C}$  for simplicity in their practical application may require some method, such as the use of chemical additives, to increase the diffusion rate of the reaction product within the cathode.

c. The Effect of Cathode Current-Collector Porosity and Pore Size on Lithium/Sulfur Cell Performance

Experiments were conducted to determine the effect of cathode current-collector porosity and mean pore diameter (usually determined by pressure-drop measurements) on capacity density. The cell design used in these studies is shown in Figure 7. This cell configuration differed from most of the other configurations that were used in that an  $\text{Al}_2\text{O}_3$  cloth ( $0.038 \text{ cm}$  thick, Union Carbide Corporation product designation ALK-15) was placed between the anode and cathode to allow minimization of the interelectrode distance while preventing short-circuiting of the two electrodes. This method allowed the interelectrode distance to be as small as  $0.3 \text{ cm}$ . The aluminum oxide cloth was attacked by lithium; consequently, these experiments were completed within eight hours or less. Voltage-capacity density and overvoltage data were gathered for this cell geometry using seven Feltmetal cathode current collectors having various porosities and pore sizes. The cells were operated at a temperature of  $375^\circ\text{C}$  and a current density of  $1.4 \text{ A/cm}^2$ . The electrolyte was the  $\text{LiF-LiCl-LiI}$  eutectic. The results are presented in Table II. The overvoltage contribution, *i.e.*, the difference between reversible emf and that available to do work in the system, due to diffusion ( $\eta_d$  [diffusion overvoltage] = open-circuit voltage-IR free voltage) and resistance ( $\eta_r$  [resistance overvoltage] = IR free voltage-terminal voltage) indicate that the total overvoltage and both components of overvoltage decrease with increasing porosity of the stainless steel Feltmetal cathode current collector up to at least 80% porosity. This is consistent with earlier but less detailed experiments on lithium/sulfur cells.<sup>(27)</sup> By coincidence  $\eta_d$  and  $\eta_r$  are identical, within experimental error, at  $1.4 \text{ A/cm}^2$ . The data of Table II were obtained under the condition of  $0.05 \text{ A-hr/cm}^2$  discharged. These results show that both the diffusion and resistance overvoltages in Feltmetal cathode current collectors operated at  $1.4 \text{ A/cm}^2$  are significant over a wide

Table I. Effect of Temperature on Lithium/Sulfur Cell Performance

Anode: Lithium

Cathode: Sulfur

Electrolyte: LiBr-RbBr eutectic salt (m.p.  $\sim 270^{\circ}\text{C}$ )

Interelectrode distance: 1 cm

Cell No.	Current Collector	Temp. ( $^{\circ}\text{C}$ )	Theoretical Capacity Density ( $\text{A-hr/cm}^2$ )	Current Density ( $\text{A/cm}^2$ )	Capacity Density Above 1 V ( $\text{A-hr/cm}^2$ )	Short Circuit Current Density ( $\text{A/cm}^2$ )	Open-Circuit Voltage (V)
21	Huyck	355	0.73	0.46	0.119	6.5	2.3
	Feltmetal	365		0.34			
	80% Porosity	364		1.03			
	29 $\mu$ pore size	363		0.34			
22	Huyck	385	0.99	1.03	0.052	-	2.3
	Feltmetal 80% porosity 29 $\mu$ pore size						
25	Mo Foam	350	0.42	0.33	0.056	8.5	2.3
	75% porosity	400		0.33			
	30 $\mu$ pore size	360		1.03			
		405		1.03			
		390		2.8			

Figure 6. Effect of Temperature on Lithium/Sulfur Cell Performance

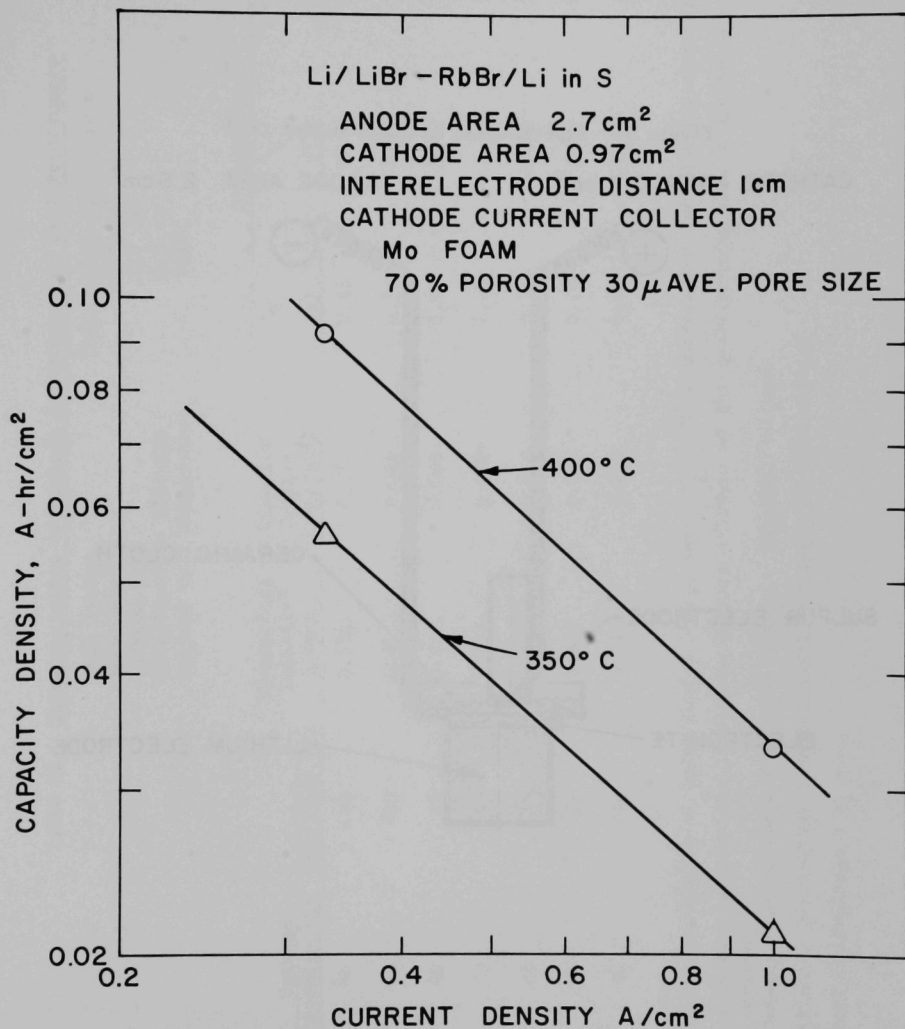


Figure 7. Experimental Lithium/Sulfur Cell

CATHODE AREA  $0.71\text{cm}^2$

ANODE AREA  $2.6\text{cm}^2$

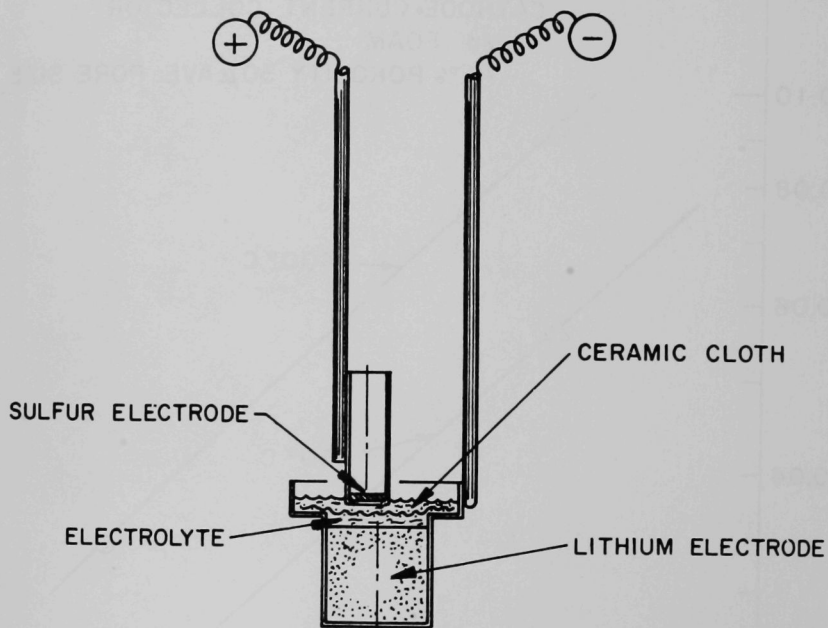


Table II. Characteristics of Cathode Structures and Cell Performance

Cell System	Li/LiF-LiCl-LiI/Li in S
Anode Area	2.6 cm <sup>2</sup>
Cathode Area	0.7 cm <sup>2</sup>
Interelectrode Distance	0.3 cm
Typical Cell Temperature	375°C

Material	Cathode		Theoretical Capacity <sup>a</sup> (A-hr)	Capacity Density (A-hr/cm <sup>2</sup> )	Overvoltages <sup>b</sup>		
	Porosity (%)	Pore Size (μ)			$\eta_r$ (v)	$\eta_d$ (v)	$\eta$ (v)
430 SS	80	240	0.910	0.17	0.48	0.50	0.98
430	60	100	0.657	0.096	0.75	0.60	1.35
302	40	19	0.437	0.043	1.0	0.90	1.9
302	70	19	0.767	0.096	0.46	0.45	0.91
302	60	19	0.657	0.060	0.75	0.80	1.55
302	80	29	0.910	0.260	0.38	0.40	0.78
430	80	240	0.910	0.200	0.48	0.65	1.13

<sup>a</sup> Based on the conversion of total sulfur charge into Li<sub>2</sub>S. No consideration was made for evaporation losses.

<sup>b</sup> These overvoltages were calculated from IR-free voltages of the cells running at 1 A discharge after 0.033 A-hr operation.

$\eta_r$  = resistance overvoltage = IR-free voltage - terminal voltage

$\eta_d$  = diffusion overvoltage = open-circuit voltage - IR-free voltage

$\eta$  = total overvoltage =  $\eta_r + \eta_d$

range of porosities and pore sizes, and that porosity has a more significant influence on overvoltage than mean pore size, higher porosities (up to 80%) yielding lower overvoltages.

The capacity densities are reported as a function of fractional porosity in Figure 8, which shows that the highest capacity densities were achieved with the 80% porosity Feltmetal. The capacity density was not very sensitive to mean pore size, but higher capacity densities were achieved with the smaller pore size ( $29 \mu$  vs  $240 \mu$ ) at the high porosities. Some previously reported results<sup>(27)</sup> indicate that 90% porous stainless steel Feltmetal current collectors show higher overvoltages than the 80% porosity current collector, but about the same capacity densities ( $0.3 \text{ A-hr/cm}^2$ ); therefore, it is reasonable to expect that the optimum porosity for a stainless steel Feltmetal current collector is near 80%, and the optimum pore size is below  $240 \mu$ .

d. Relationship Between Current Density and Capacity Density

The relationship between current density and the capacity density that can be obtained above a useful cut-off voltage (such as 1 V) is an important aspect of cell performance. Figure 9 shows the capacity density as a function of current density for several different current-collector materials and designs. The effect of current-collector geometry on cell performance will be discussed more fully in the following section.

The data of Figure 9 were obtained with a cell geometry similar to that shown in Figure 1. All cells were operated similarly except that the current-collector structure was changed between tests. If the diffusion of products into the sulfur cathode obeyed the laws of semi-infinite linear diffusion, the curves of Figure 9 would have a slope of minus one; the experimental data have slopes between -0.5 and -1.4. It is clear from Figure 9 that the structure (porosity, pore size and distribution, type of structure) has a strong influence on the capacity density available at a given current density. The results in Figure 9 reflect the conflicting requirements placed upon a well-designed current collector. The current collector must provide ready accessibility of electrons at the reaction sites but must not unduly interfere with the diffusion of reaction products away from the cathode-electrolyte interface.

e. Effect of Current-Collector Geometry on Lithium/Sulfur Cell Performance

Because of the demonstrated importance of a well-designed current collector in providing increased cell performance, many cells were operated with the objective of studying the relationship between current-collector design and cell performance. In these tests

Figure 8. Relationship between the Porosity of the Cathode Current Collector and the Capacity Density of Lithium/Sulfur Cells

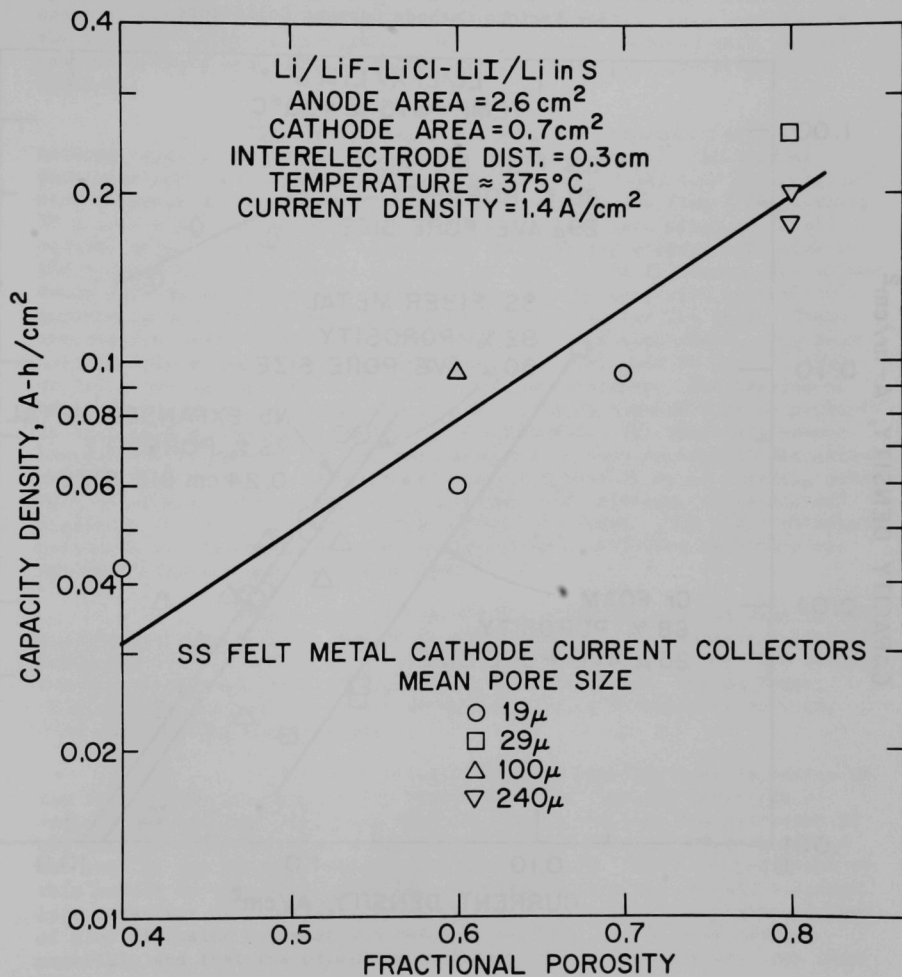
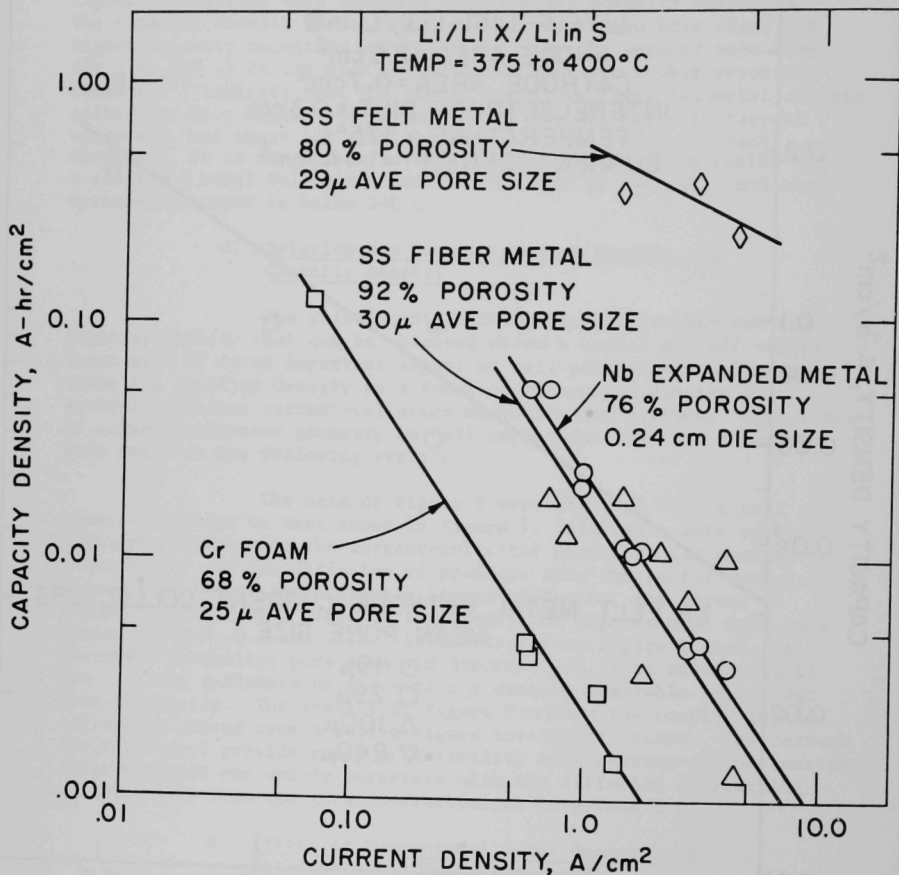


Figure 9. Capacity Density-Current Density Relationship  
for Various Cathode Current Collectors



the pore size, porosity, material, method of fabrication, and thickness of the cathode current collector were varied and the cell performance was evaluated. The relationship between mean pore diameter, porosity, and cell performance (especially capacity density) was discussed above (part c of this section). Figure 9 shows that the current density-capacity density relationship for lithium/sulfur cells is a function of the current-collector structure. Data from cells operated with varying cathode current collector materials and structures are presented in Table III.

The data of Table III show the pronounced effect of cathode current-collector structure on capacity density. At current densities near  $0.5 \text{ A/cm}^2$ , capacity densities from  $0.003$  to  $0.143 \text{ A-hr/cm}^2$  were obtained as the structure was varied. Molybdenum foam (75% porosity,  $30 \mu$  pore size) and Feltmetal (80% porosity,  $29 \mu$  pore size) performed equally well. It should be noted that although the average pore size of the molybdenum foam is about the same as that of the Feltmetal, the molybdenum foam is substantially different because the pore size distribution appears to be much narrower for the Feltmetal than for the foam. These observations are visual; no quantitative data have been taken. The foam used in Cell 27 was of a higher porosity than that used in Cell 26 (82% vs 75%), but information on pore size is not available. The results of Cells 7, 26 and 27 indicated, in general, that molybdenum foam is probably as effective a current collector as is Feltmetal. The small difference between the porosities of the foams appeared to have no significant effect on cell performance. These results are considered to be encouraging since many materials, such as beryllium, niobium, and chromium, which are not available as Feltmetal, can be fabricated into foams. The other materials tested do not appear to be as effective current-collector materials as are the Feltmetal and molybdenum foam.

The effect of cathode thickness on capacity density was investigated using three similar  $\text{Li/LiBr-RbBr/Li}$  in S, liquid-electrolyte cells operated at  $400^\circ\text{C}$ . The difference in the cells was that the cathode current collectors (Type 302 stainless steel Feltmetal, 80% porosity,  $29 \mu$  average pore size,  $0.7 \text{ cm}^2$  surface area) had thicknesses of  $0.16$ ,  $0.32$  and  $0.48 \text{ cm}$ , respectively.

The current density-capacity density characteristics of the three cells are compared in Figure 10. The capacity densities at various current densities were similar, indicating that the thickness of the current collector had no significant effect upon the performance of the cell in the range of thicknesses investigated. The interpretation of this result is that the sulfur that was remote from the cathode-electrolyte interface did not participate in the cell reaction, probably because of slow diffusion rates of the reaction products in the bulk cathode material, and that the effective thickness of the cathodes was less than  $0.16 \text{ cm}$ .

The percentage of theoretical capacity density obtained in these cells was inversely related to the cathode thickness, with the

Table III. Effect of Cathode Current Collector Structure  
on Lithium/Sulfur Cell Performance

Anode: Lithium

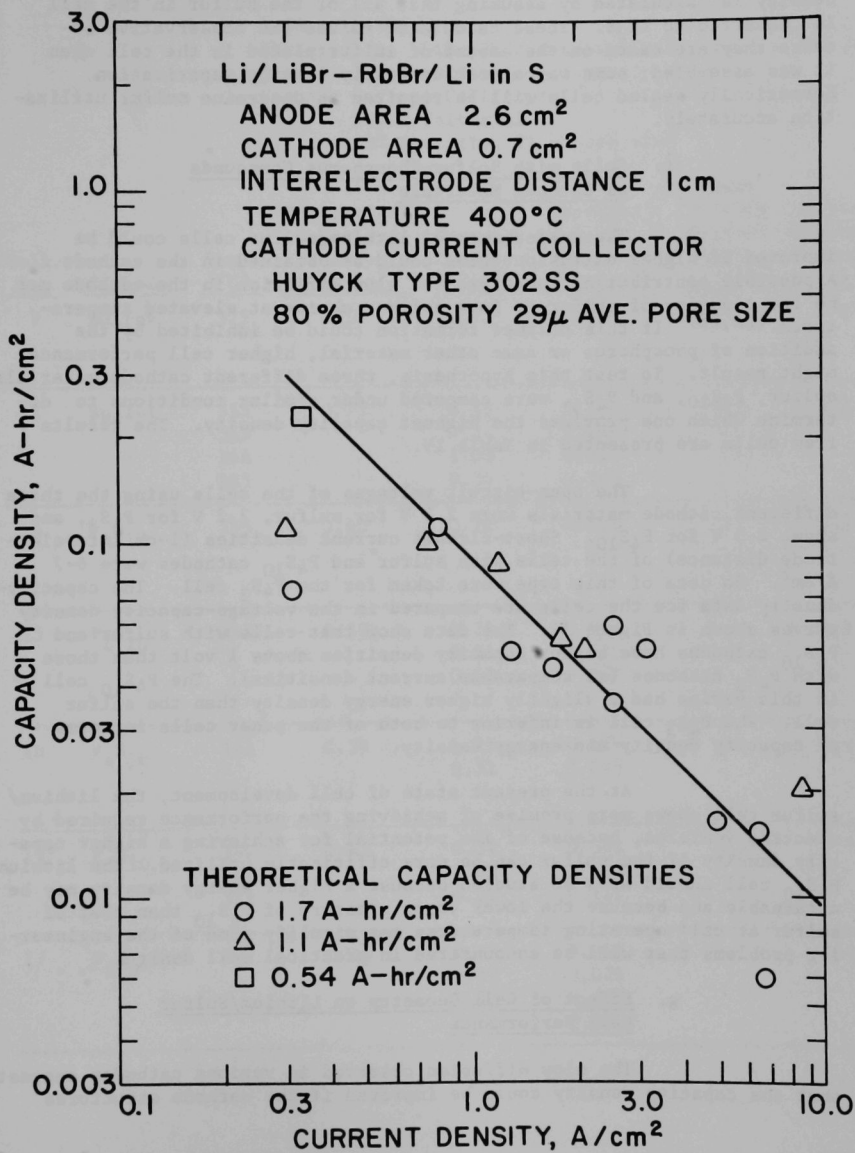
Cathode: Sulfur

Electrolyte: LiBr-RbBr eutectic salt (m.p.  $\sim 270^{\circ}\text{C}$ )

Interelectrode Distance: 1 cm

Cell No.	Cathode Current Collector	Temp. ( $^{\circ}\text{C}$ )	Theoretical Capacity Density ( $\text{A-hr/cm}^2$ )	Current Density ( $\text{A/cm}^2$ )	Capacity Density Above 1 V ( $\text{A-hr/cm}^2$ )
7	Huyck Feltmetal 80% Porosity 29 $\mu$ pore size	375	0.50	0.57	0.114
9	Brunswick Fibermetal 85% Porosity 40 $\mu$ pore size	375	0.26	0.41	0.048
26	Mo Foam 75% Porosity 30 $\mu$ pore size	400 400	0.46	0.44 0.88	0.143 0.051
27	Mo Foam 82% Porosity	385	0.62	0.43 0.85 1.39	0.121 0.060 0.023
-	Nb Expanded Mesh 76% Porosity 0.24 cm die size	385	1.2	0.58	0.005
1	Cr Foam 68% Porosity 25 $\mu$ pore size	385	0.43	0.60	0.004
3	Brunswick Fibermetal 92% Porosity 30 $\mu$ pore size	385	0.32	0.44	0.003

Figure 10. Effect of Cathode Thickness on Capacity Density-Current Density Characteristics of Lithium/Sulfur Cells



thinnest (0.16-cm) cathode structure yielding the highest value of 43% of the theoretical capacity density. The theoretical capacity density is calculated by assuming that all of the sulfur in the cell is converted to  $\text{Li}_2\text{S}$ . These calculated values are conservative because they are based on the amount of sulfur placed in the cell when it was assembled; some was almost certainly lost by vaporization. Hermetically sealed cells will be required to determine sulfur utilization accurately.

f. Cells with Sulfur-Phosphorus Compounds as Cathode Materials

The performance of lithium/sulfur cells could be improved if higher diffusion rates could be obtained in the cathode. A possible contributing factor to the slow diffusion in the cathode may be the tendency of sulfur to form polymer chains at elevated temperatures. (26,28) If this polymer formation could be inhibited by the addition of phosphorus or some other material, higher cell performance might result. To test this hypothesis, three different cathode materials, sulfur,  $\text{P}_4\text{S}_{10}$ , and  $\text{P}_4\text{S}_3$ , were compared under similar conditions to determine which one provides the highest capacity density. The results from cells are presented in Table IV.

The open-circuit voltages of the cells using the three different cathode materials were 2.3 V for sulfur, 2.2 V for  $\text{P}_4\text{S}_3$ , and about 2.5 V for  $\text{P}_4\text{S}_{10}$ . Short-circuit current densities (1-cm interelectrode distance) of the cells with sulfur and  $\text{P}_4\text{S}_{10}$  cathodes were 6-7  $\text{A}/\text{cm}^2$ . No data of this type were taken for the  $\text{P}_4\text{S}_3$  cell. The capacity density data for the cells are compared in the voltage-capacity density curves shown in Figure 11. The data show that cells with sulfur and  $\text{P}_4\text{S}_{10}$  cathodes have higher capacity densities above 1 volt than those with  $\text{P}_4\text{S}_3$  cathodes (at comparable current densities). The  $\text{P}_4\text{S}_{10}$  cell in this series had a slightly higher energy density than the sulfur cell. The  $\text{P}_4\text{S}_3$  cell is inferior to both of the other cells in terms of capacity density and energy density.

At the present state of cell development, the lithium/sulfur cell shows more promise of achieving the performance required by electric vehicles, because of its potential for achieving a higher capacity density if the sulfur can be more efficiently utilized. The lithium/ $\text{P}_4\text{S}_{10}$  cell should also be studied because a higher energy density may be attainable and because the lower vapor pressure of  $\text{P}_4\text{S}_{10}$  than that of sulfur at cell operating temperatures may simplify some of the engineering problems that will be encountered in practical cell design.

g. Effect of Cell Geometry on Lithium/Sulfur Cell Performance

The slow diffusion observed in various cathodes suggests that the capacity density could be improved if the cathode structures

Table IV. Comparison of Lithium/Sulfur, Lithium/P<sub>4</sub>S<sub>10</sub> and Lithium/P<sub>4</sub>S<sub>3</sub> Cells

Anode: Lithium

Electrolyte: LiBr-RbBr eutectic salt (m.p. ~ 270°C)

Interelectrode Distance: 1 cm

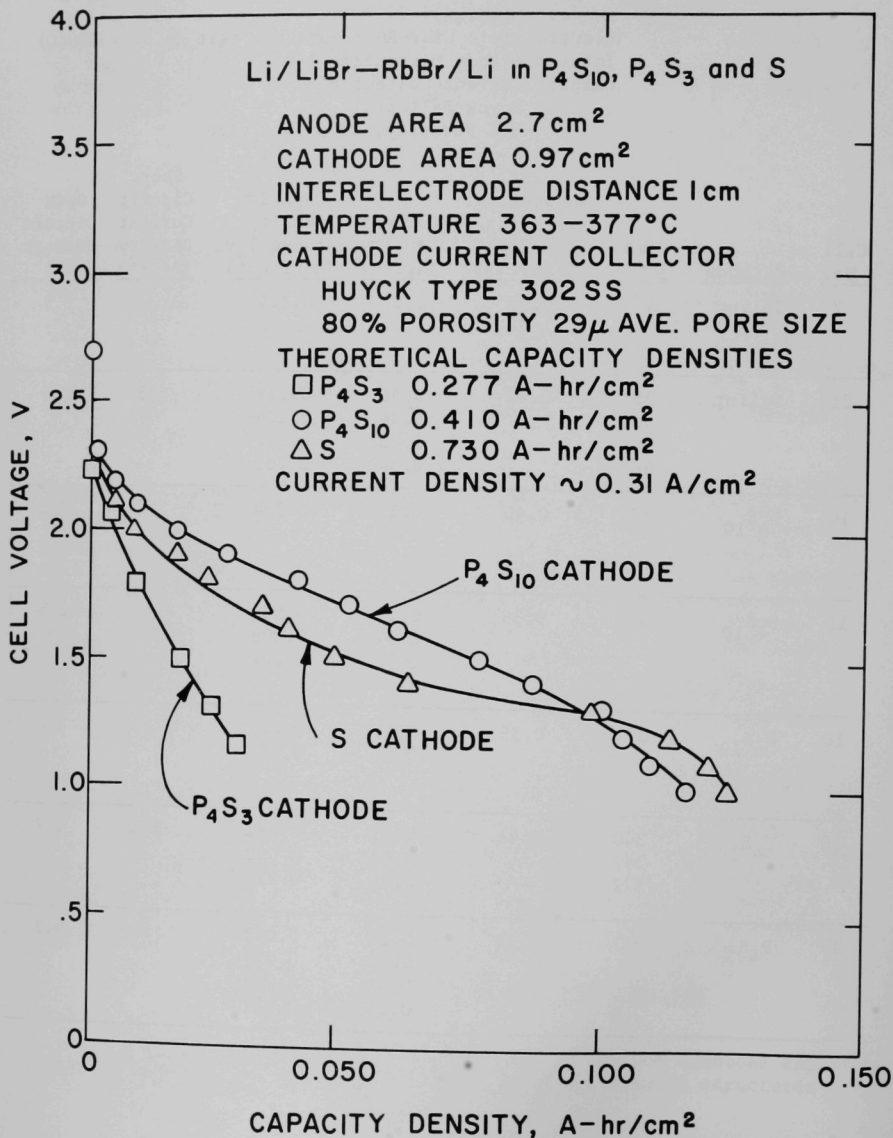
Cathode Current Collector

Huyck Feltmetal

80% Porosity, 29 μ pore size

Cell No.	Cathode	Temp. (°C)	Theoretical Capacity Density (A-hr/cm <sup>2</sup> )	Current Density (A/cm <sup>2</sup> )	Capacity Density Above 1 V (A-hr/cm <sup>2</sup> )	Short Circuit Current Density (A/cm <sup>2</sup> )	Open Circuit Voltage (V)
7	Sulfur	375	0.50	0.57	0.114	-	2.3
21	Sulfur	355	0.73	0.46	0.119	6.5	2.3
		365		0.34	0.124		
		364		1.03	0.022		
		363		0.34	0.103		
14	P <sub>4</sub> S <sub>10</sub>	375	0.40	0.12	0.074	-	2.5
15	P <sub>4</sub> S <sub>10</sub>	368	0.39	0.21	0.015	-	2.5
				0.31	0.009		
				0.52	0.007		
16	P <sub>4</sub> S <sub>10</sub>	373	0.39	0.21	0.069	-	2.4
				0.31	0.073		
19	P <sub>4</sub> S <sub>10</sub>	340	0.41	0.31	0.082	6.2	2.7
		357		0.60	0.092		
		372		0.31	0.116		
17	P <sub>4</sub> S <sub>3</sub>	377	0.28	0.13	0.053	-	2.2
				0.33	0.029		
				0.41	0.027		
				0.64	0.037		

Figure 11. Comparison of Voltage-Capacity Density Data for  
Lithium/Sulfur, Lithium  $P_4S_{10}$  and Lithium/ $P_4S_3$  Cells



could be designed with a high surface-to-volume ratio. A substantially different cell design intended to increase the sulfur-electrolyte interfacial area in a given volume is shown in Figure 12. It contained four pieces of Huyck Type 302 SS Feltmetal (11 x 11 x 1.6 mm) impregnated with sulfur. These four cathode parts were sandwiched between five similarly-sized pieces of Feltmetal impregnated with electrolyte to form a laminated cathode structure. The cathode assembly was immersed in the liquid electrolyte to a depth of  $\sim 3$  mm. It was expected that the electrolyte-filled Feltmetal would wick up any additional salt that was required. With this design, the projected area of the cathode, *i.e.*, the cathode-electrolyte surface directly facing the anode, was  $1.58 \text{ cm}^2$ . This design has several advantages over the previous designs, the major benefit being the availability of both sides of the cathode current collector layers as reaction surfaces. The voltage-current density data for this cell are shown in Figure 13. A short-circuit current density of  $6.6 \text{ A/cm}^2$  was obtained with this cell. This value is similar to that obtained with the other cell designs, as would be expected, since the same electrolyte and interelectrode distance were used.

Voltage capacity-density data are presented in Figure 14. At a current density of  $0.32 \text{ A/cm}^2$ , a capacity density of  $0.29 \text{ A-hr/cm}^2$  was measured. The current density-capacity density behavior was similar to that observed with the previous cell designs. A factor of two ( $0.32$  to  $0.63 \text{ A/cm}^2$ ) increase in current density reduced the capacity density (above 1 V) from  $0.29$  to  $0.14 \text{ A-hr/cm}^2$ , about a factor of two.

The percent of theoretical capacity obtained in this cell (above 1 V) varied from 12 to 24%, depending upon the current density. This is a higher utilization than has been obtained previously (about 22% at low current densities) but was not the factor of two increase hoped for since both sides of the current collector are reaction surfaces. This suggests that the design may not have been optimized to provide adequate electrolyte to both sides of the current collector.

A cell of this design was discharged as far as practicable to determine the maximum amount of lithium that could be reacted with the sulfur. This was accomplished by discharging the cell to zero voltage, allowing diffusion to proceed and the cell to recover on open circuit, and discharging again to zero voltage. This procedure was repeated 19 times, at which point  $0.67 \text{ A-hr/cm}^2$  had been withdrawn from the cell. This corresponds to about 52% sulfur utilization based on conversion to  $\text{Li}_2\text{S}$  of all sulfur initially charged to the cell. Some sulfur was probably lost from the cell, since shortly after insertion into the electrolyte, vapors emanating from the vicinity of the cell were observed. Efforts were made to condense the vapors for analysis but the vaporization ceased before preparations for sample collection could be completed.

These cells demonstrated that the use of laminated cathode structures is feasible with lithium/sulfur cells. Other cell

Figure 12. Laminated-Cathode Lithium/Sulfur Cell

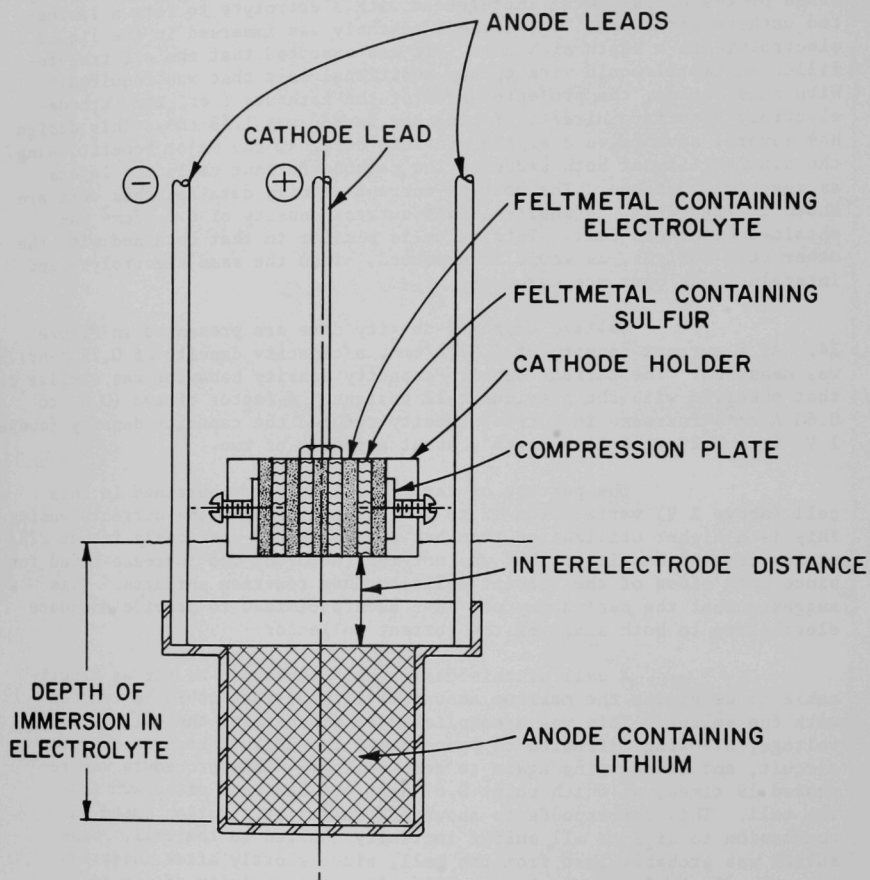


Figure 13. Voltage-Current Density Data for Lithium/Sulfur  
Cell with Laminated Cathode

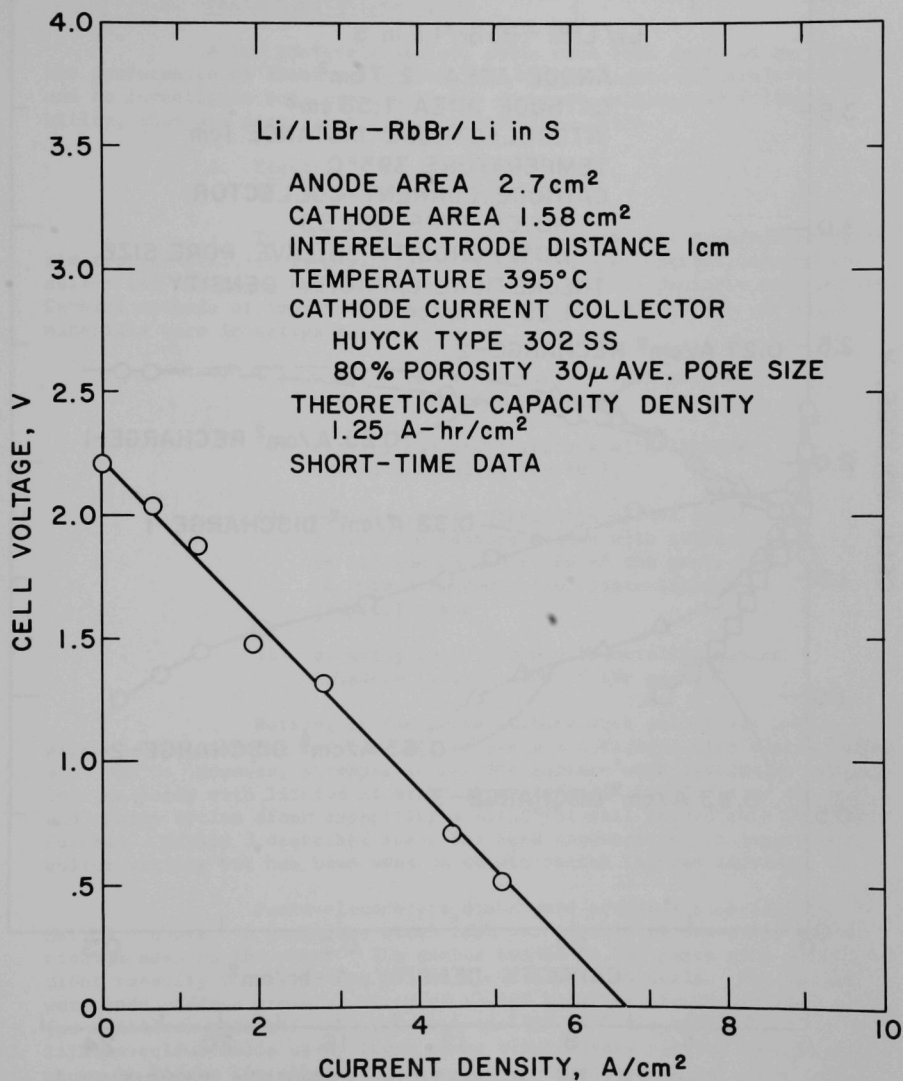
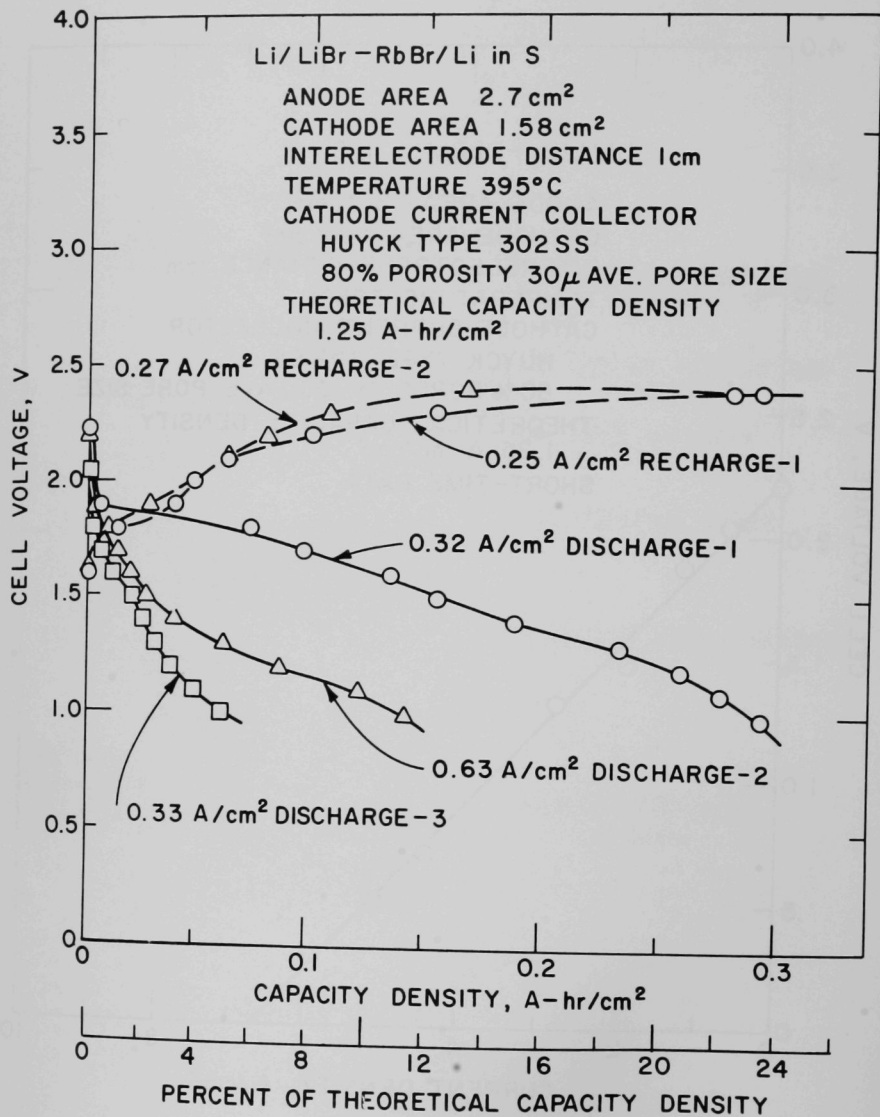


Figure 14. Voltage-Capacity Density Data for Lithium/Sulfur Cell with Laminated Cathode



configurations incorporating both the laminated cathode design and sealing for containment of sulfur vapors will be tested.

## 2. Paste-Electrolyte Cells

A few paste-electrolyte cells have been operated to compare the performance of these cells with that of the liquid-electrolyte cells and to investigate some problems, such as paste wetting and filler stability, that are peculiar to paste-electrolyte cells.

### a. Electrical Performance (V. A. Maroni, H. Shimotake)

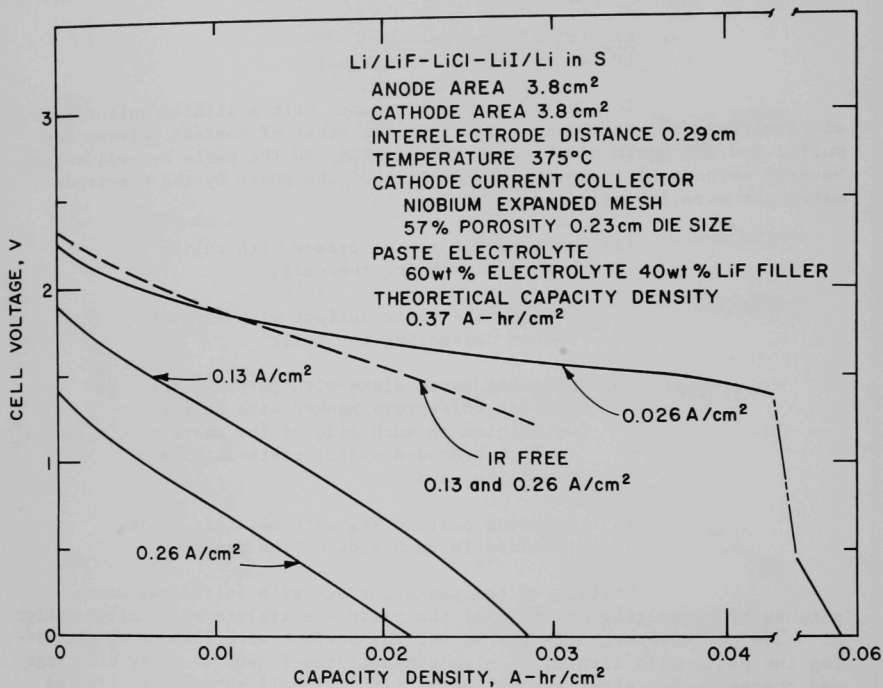
To achieve high performance with a lithium/sulfur paste-electrolyte cell, it is essential that the areas of contact between the sulfur and the paste and between the lithium and the paste be well wetted. Several methods of improving the wetting of the paste by the electrode materials were investigated:

- (1) wetting the paste surface with sulfur before assembling the cell;
- (2) wetting the paste surface with lithium before assembling the cell;
- (3) pressing paste disks with porous metal current collectors soaked with sulfur or lithium on each side of the paste to form a bonded sulfur-paste-lithium composite; and
- (4) pressing paste disks with metallic meshes imbedded in each side of the paste.

Wetting of the paste surface with sulfur was accomplished by contacting one face of the paste electrolyte with molten sulfur at  $\sim 300^{\circ}\text{C}$ . However, attempts to wet the surface with lithium by contacting the paste with lithium at high temperatures ( $> 400^{\circ}\text{C}$ ) or by discharge and charge cycles after assembling a  $\text{Li}/\text{Li}^+/\text{Li}$  cell showed only limited success. Method 3 described above has been unsuccessful in regard to sulfur wetting but has been used to obtain better lithium wetting.

Paste-electrolyte disks were prepared according to Method 4 above. A stainless steel mesh was pressed on one side, and a niobium mesh on the other. The meshes bonded to the paste with sufficient tenacity to permit use of the electrolytes in cells. The pastes were made under a pressing force of 12,700 kg after mixing powdered  $\text{LiF}$  (as a filler) with  $\text{LiF-LiCl-LiI}$  eutectic (40 wt % electrolyte). The lithium-sulfur cells using these paste electrolytes yielded the results shown in Figure 15. Short-circuit current densities of  $0.9 \text{ A}/\text{cm}^2$  and

Figure 15. Voltage-Capacity Density Data for Lithium/Sulfur Cell  
with a Paste Electrolyte



capacity densities of up to 0.05 A-hr/cm<sup>2</sup> (above zero voltage) were obtained. The pastes showed deformation, but the color remained white-to-gray after about 24 hours of operation. The lithium electrode showed good adhesion to the paste, but the sulfur electrode, consisting of four niobium mesh layers, was dry perhaps due to evaporation of the sulfur.

A second lithium/sulfur cell with a paste electrolyte consisting of 60 wt % LiBr-RbBr eutectic and 40 wt % LiAlO<sub>2</sub> filler was operated at 400°C. No prewetting procedures were used with this cell. During the first six hours of operation, short-circuit current densities of about 0.8 A/cm<sup>2</sup> were obtained; the open-circuit voltages were in the range of 2.2 to 2.5 V. After the cell had been on open circuit overnight, the internal resistance increased considerably and its performance decreased sharply. Testing was terminated after 24 hours. Pertinent data on this cell include a maximum short-circuit current density of 0.84 A/cm<sup>2</sup>, a maximum power density of 0.52 W/cm<sup>2</sup>, and capacity densities of 0.010 A-hr/cm<sup>2</sup> (at 0.06 A/cm<sup>2</sup>, above 1.6 V) and 0.018 A-hr/cm<sup>2</sup> (at 0.225 A/cm<sup>2</sup>, above zero voltage). The theoretical capacity density of the cell was 0.9 A-hr/cm<sup>2</sup>; about 2% of this value was achieved. These results indicate that the power density of the cell was adequate but that the capacity density must be increased before lithium/sulfur cells with paste electrolytes become practical. The short life of this cell is not surprising since the Type 302 stainless steel used as the cathode current collector is not corrosion-resistant to lithium-sulfur mixtures, and it probably deteriorated rapidly in service. Cathode current collectors of more corrosion-resistant materials are required to permit longer cell life.

b. Filler Stability  
(A. K. Fischer, F. L. Ferry)

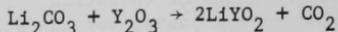
Research on paste-electrolyte fillers for the lithium/sulfur cell was concerned with the synthesis of the materials Li<sub>2</sub>ZrO<sub>3</sub>, LiYO<sub>2</sub>, and MgAl<sub>2</sub>O<sub>4</sub>, and with stability tests in molten sulfur of  $\gamma$ -LiAlO<sub>2</sub>, AlN, LiYO<sub>2</sub>, MgO, ThO<sub>2</sub>, MgAl<sub>2</sub>O<sub>4</sub>, and CaO.

The compound Li<sub>2</sub>ZrO<sub>3</sub> was prepared by heating a uniform mixture of Li<sub>2</sub>CO<sub>3</sub> and ZrO<sub>2</sub> powders at successively higher temperatures, ranging from 600 to 720°C, over a period of eleven days. During this time, the reaction mixture lost weight due to CO<sub>2</sub> evolution according to the equation:



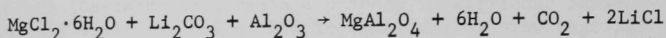
The product was washed with water, dried, and weighed. The yield was 94% of the theoretical amount expected on the basis of the above equation. X-ray diffraction analysis supported the conclusion that Li<sub>2</sub>ZrO<sub>3</sub> was formed.

The compound  $\text{LiYO}_2$  was prepared according to the reaction:



by heating the reactants at  $800^\circ\text{C}$  for one day. The product was obtained in greater than 90% yield after being washed with water. X-ray diffraction analysis showed that the product was  $\text{LiYO}_2$  with only a minor amount of  $\text{Y}_2\text{O}_3$  present.

The spinel,  $\text{MgAl}_2\text{O}_4$ , was prepared by the reaction:

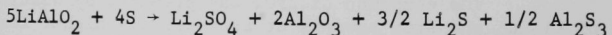


The powdered reactants, mixed and compressed into a pellet, were heated at  $90^\circ\text{C}$  for three days. The product was washed free of carbonate, analyzed by X-ray diffraction, and found to contain  $\text{MgAl}_2\text{O}_4$  as the major component. One weak line in the X-ray diffraction pattern could not be assigned to  $\text{MgAl}_2\text{O}_4$ .

Three sets of sulfur stability tests were conducted.\* In the first set,  $\gamma\text{-LiAlO}_2$ ,  $\text{CaO}$ ,  $\text{ThO}_2$  and  $\text{MgO}$  were the test fillers. These materials, as powders, were mixed with sulfur and heated at  $375^\circ\text{C}$  in Pyrex tubes in a helium atmosphere for five days. At the end of that time, the  $\text{ThO}_2$  showed considerable browning and blackening and obviously had reacted. The  $\text{CaO}$  had become tan in color; at calcining temperature, which is higher than the temperature used here, the reaction



is known to occur.<sup>(29)</sup> Presumably, a similar reaction occurred in our tests. The  $\gamma\text{-LiAlO}_2$  and  $\text{MgO}$  emerged apparently unattacked, except that the  $\text{MgO}$  showed a slight sign of darkening. These two samples were washed with  $\text{CS}_2$  and analyzed by X-ray diffraction. In the  $\text{MgO}$  sample, no reaction products from  $\text{MgO}$  (such as  $\text{MgS}$  or  $\text{MgSO}_4$ ) were found, but in the  $\text{LiAlO}_2$  sample, a possible, very minor, amount of  $\text{Li}_2\text{S}$  was detected. A reaction between  $\text{LiAlO}_2$  and sulfur that would produce  $\text{Li}_2\text{S}$  can be conceived of, at least on paper:



For this reaction,  $\Delta H_{298}^\circ = -22 \text{ kcal}$ , or about  $-4 \text{ kcal}$  per mole of  $\text{LiAlO}_2$ .<sup>(30)</sup>

In the second set of sulfur stability tests, the filler materials were  $\gamma\text{-LiAlO}_2$ ,  $\text{MgO}$  (for a repeated examination),  $\text{AlN}$ , and  $\text{LiYO}_2$ .

\*  $\text{Li}_2\text{ZrO}_3$  was not included in the sulfur stability tests because it was found not to be stable toward lithium.

On thermodynamic grounds, AlN promised great stability toward lithium, but its stability toward sulfur was of interest, too. Test conditions were the same as in the first set of experiments, but the duration of the test was seven days. It was found that AlN and LiYO<sub>2</sub> had reacted. The MgO and LiAlO<sub>2</sub> again survived without sign of major change except for a few dark spots on the tube walls, which might have been droplets of highly polymerized sulfur. These materials were washed with CS<sub>2</sub> and analyzed by X-ray diffraction. Only the parent materials were found. (31)

In the final set of sulfur stability tests, LiAlO<sub>2</sub>, MgO, and MgAl<sub>2</sub>O<sub>4</sub> were examined. Test conditions were the same as in the second set. The products were not washed with CS<sub>2</sub> this time to avoid prolonged exposure to air and possible hydrolysis of reaction products, if any. X-ray diffraction analysis showed no foreign materials—only sulfur and the original filler material. This result was interesting in the case of MgAl<sub>2</sub>O<sub>4</sub> because this material seemed to show a greenish discoloration at the end of the experiment; the greenishness might have resulted from some unknown aspect of the sulfur polymerization that occurs at high temperature.

These tests established that LiAlO<sub>2</sub>, MgO, and MgAl<sub>2</sub>O<sub>4</sub> might be acceptable filler materials for paste electrolytes in lithium-sulfur cells. The somewhat conflicting data obtained with LiAlO<sub>2</sub> might be the result of differences in the test duration. It is possible that, given longer exposure, LiAlO<sub>2</sub> might react with sulfur. Since prolonged exposure would occur in a practical lithium/sulfur battery, much longer stability tests will be needed, ones perhaps six months in duration, to establish the most practical filler materials for cell application. Lithium aluminate is being used in most of the preliminary cell tests because methods of producing this material in the small particle sizes are known.

#### B. Results of Corrosion Tests

(M. L. Kyle, P. W. Krause, F. J. Martino)

The results of the corrosion-testing program can best be described by reviewing the results for three different classes of materials: (1) rigid electrical insulators, (2) pliable electrical insulators, (3) electrically-conducting materials.

##### 1. Rigid Electrical Insulators

Rigid electrical insulators are used in paste-electrolyte cells for electrical isolation of the anode and cathode housings. These insulators must be resistant, in this application, to attack by molten lithium, the molten-salt electrolyte, and molten sulfur. Resistance to attack by lithium is the most difficult condition to meet because many of the more common insulators such as MgO, ZrO<sub>2</sub>, Al<sub>2</sub>O<sub>3</sub>, Pyrex, and quartz, are oxides which are readily reduced by lithium. (32)

Table V presents the results of dynamic isothermal capsule tests that were conducted to determine the corrosion-resistance of

Table V. Corrosion of Electrical Insulators  
by Molten Lithium-Sulfur Mixtures

Temperature: 375°C  
 Static Immersion Tests  
 Composition: 20 at.% Lithium,  
 80 at.% Sulfur

<u>Material</u>	<u>Exposure Period (hr)</u>	<u>Corrosion Rate (mm/yr)</u>	<u>Remarks</u>
BN <sup>a</sup>	101	< 0.6	No detectable attack
BN	331	0.14	Sample darkened
Y <sub>2</sub> O <sub>3</sub>	311	0.033	Slight weight loss
Y <sub>2</sub> O <sub>3</sub>	331	0.65	Weight gain
MgO <sup>b</sup>	305	1.1	Severe attack

<sup>a</sup> Tested in pure sulfur; no lithium present.

<sup>b</sup> Single crystal.

various electrical insulators to molten lithium-sulfur mixtures at 375°C. Boron nitride performed well in two tests. The shorter corrosion test showed no detectable attack, but, under increased exposure time, a sample showed surface darkening and slight weight loss. These effects are attributed to the reaction between lithium and the  $B_2O_3$  contained in the BN. This material is believed to be an adequate insulator for use in lithium/sulfur cells, at least those with an anticipated lifetime of several hundred hours. Yttria showed somewhat different performance in two exposures. Almost no evidence of attack was found after the first exposure, but when a duplicate test was made, the  $Y_2O_3$  specimen increased in weight but visually appeared to be unaffected. This weight increase was not accompanied by any measurable change in size or decrease in insulating properties. The reason for the weight gain is unexplained but it might have resulted from the inclusion of such materials as  $Li_2O$  in the pores of the sample. It is still believed that this material may be an adequate insulator for lithium-sulfur cells. Magnesia was severely attacked by lithium-sulfur mixtures, and no further work with this material is planned.

The corrosion resistance of  $BeO$  to molten lithium was measured in an 1168-hr immersion test at 375°C. The average corrosion rate over the duration of the test was 0.011 mm/yr (0.44 mil/yr) and visual inspection showed a slight greying of the almost translucent material but very little evidence of any other attack. This result is presented in Figure 16 where it is compared with data obtained previously<sup>(32)</sup> for the resistance of electrically insulating materials to lithium. This is the most lithium-resistant insulator tested to date.

Three distinct types of  $BeO$  have been tested, the hot-pressed, high-purity grade tested in this experiment, and both re-crystallized and commercial grades tested previously. The corrosion of these samples has varied considerably from 12 mm/yr for the commercial grade to 0.011 mm/yr for the hot-pressed, high-purity  $BeO$ . It is obvious that the purity and method of fabrication of  $BeO$  are important variables when determining its corrosion resistance in molten lithium.

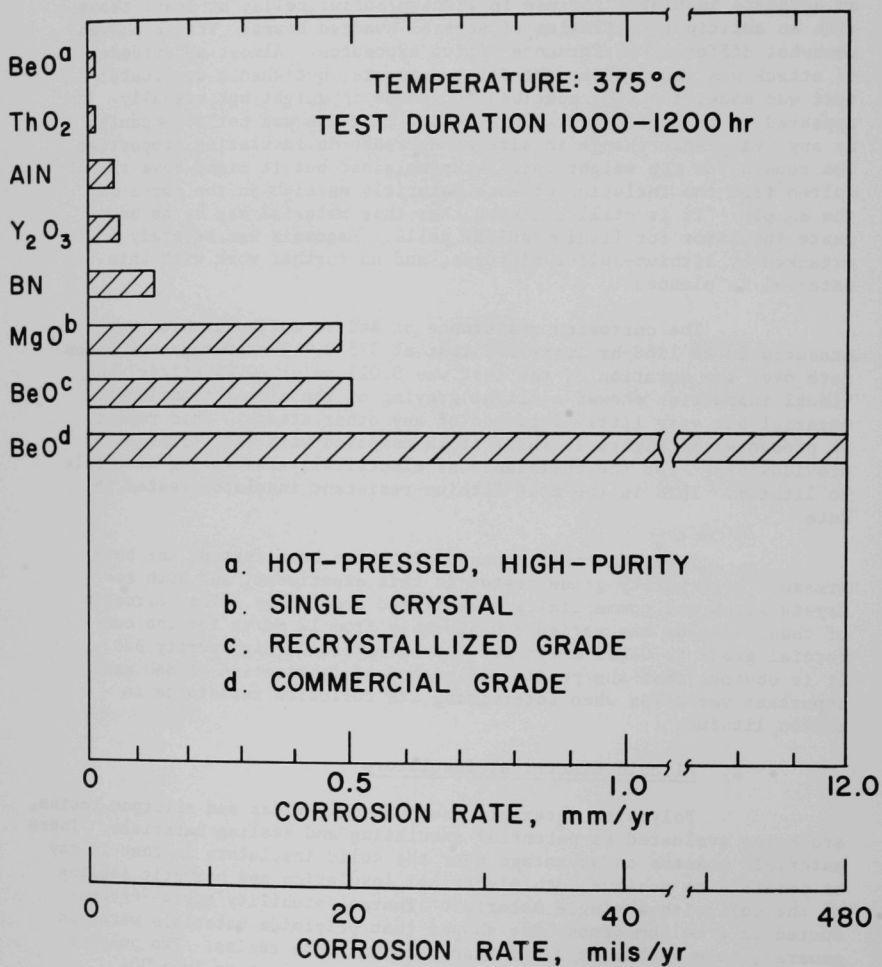
## 2. Pliable Electrical Insulators

Polymeric materials, such as polyimides and silicone resins, are being evaluated as potential insulating and sealing materials. These materials possess an advantage over the solid insulators in that it may be possible to achieve both electrical insulation and hermetic sealing of the cell with a single material. Thermal stability tests<sup>(32)</sup> conducted in a helium atmosphere showed that polyimide materials were, in general, more stable at 375°C than were silicone resins. Two polymer films, Dexsil\* and Pyre ML,<sup>†</sup> were tested as coatings on Type 304

\* Polycarboranesiloxane product of Olin Mathieson Corporation.

† Polyimide product of E. I. duPont de Nemours and Co., Inc.

Figure 16. Corrosion of Electrical Insulators by Molten Lithium



stainless steel coupons in 311-hr tests at 375°C in a 20 at.% Li-S system. Both polymer films were completely removed from the stainless steel coupons.

Other attempts were made to produce light-weight electrical insulators by forming composite structures in which  $\text{LiAlO}_2$  was used as the bulk insulator, and the desired shape was obtained through the use of a polyimide binder. One of these composites (containing two-thirds  $\text{LiAlO}_2$  and one-third Pyre ML, by weight) was exposed to molten 20 at.% lithium-sulfur mixtures, and to two molten-salt electrolytes,  $\text{LiBr-RbBr}$  and  $\text{LiF-LiCl-LiI}$ , at 375°C in 233-hr tests. This composite appeared to be somewhat resistant to the  $\text{LiF-LiCl-LiI}$  eutectic salt with the attack (1.1 mm/yr) resulting from destruction of the Pyre ML binder. The Pyre ML binder was completely destroyed in the other two samples, and a finely powdered material, apparently  $\text{LiAlO}_2$ , was recovered at the completion of the tests. This method of insulator preparation does not look promising unless more resistant binders can be discovered.

### 3. Electrically Conducting Materials

Corrosion tests of electrically conducting materials were made to identify those materials with promise for cell application as housing and current-collector materials.

#### a. Results of 100- to 300-Hour Screening Tests

Screening tests have been conducted for periods of 100 to 300 hr at 375°C in 20 at.% lithium-sulfur mixtures. Those materials that show promise in the screening tests were subjected to more extensive testing. The results of 100- to 300-hr screening tests are presented in Table VI and the chemical compositions of the materials tested are listed in Table VII.

A wide variety of stainless steels was tested. In general, the corrosion rates were less than 0.15 mm/yr. Both nickel-chromium and manganese-chromium stainless steels yielded similar results. Attack generally occurred by a surface reaction which produced an adherent electrically conductive film. In most cases, the film formation was accompanied by a weight loss of the specimen indicating ablation of at least part of the film. For the samples reported as having "+" corrosion rates, the film formation caused a weight gain of the specimen, indicating that reaction film formation probably proceeded from the original surface with little ablation.

Nickel-base alloys are more variable in their performance, as shown by the results for Hastelloy B and Monel as contrasted with the performance of Hastelloy X and Inconel 702. Inconel 702 and Hastelloy X appeared to gain their corrosion resistance through the formation of tenacious films which, in the case of Inconel 702 at least, are not electrically conductive.

Table VI. Corrosion of Metals by Molten Lithium-Sulfur Mixtures: Screening Tests

Temperature: 375°C  
Composition: 20 at.% Li-S

Test Material	Exposure Period (hr)	Corrosion Rate (mm/yr)	Remarks
<u>Stainless Steels (Ni-Cr)</u>			
2 RN 65	311	0.10	Conductive surface film.
2 RK 65	311	0.03	Conductive surface film.
2 RE 10	311	0.12	Conductive surface film.
Worthite	311	+0.07 <sup>a</sup>	Conductive surface film.
347 (2 tests)	311, 331	0.09, 0.022	Conductive surface film.
Carpenter 20	304	+0.21	Conductive surface film.
Croloy 16-1	304	+0.14	Conductive surface film.
Durimet 20	100	+0.24	Adherent film formation.
<u>Nickel-Base Alloys</u>			
Hastelloy B	309	1.93	Dissolution.
Inconel 718	100	+0.12	Adherent surface film.
Inconel 702	311	0.02	Nonconductive surface film.
Inconel 800	331	0.23	Conductive surface film.
Monel	304	3.68	Dissolution.
Hastelloy X	331	0.02	Conductive surface film.
<u>Stainless Steels (Mn-Cr)</u>			
205	309	0.05	Conductive surface film.
Tenelon	304	0.18	
<u>Other</u>			
Nb	306	0.09	
Mg (3 tests)	304, 331, 331	0.12, 0.11, 0.24	Nonconductive surface film.
Al (3 tests)	304, 331, 331	0.19, 0.02, 0.85	Nonconductive surface film.
Ti	304	0.48	
Cr	100, 328	0.01,+0.17	Conductive surface film.
Mo	100	0.01	No detectable corrosion.
LT-1	101	0.03	Al <sub>2</sub> O <sub>3</sub> reduction.
Zircaloy-2	101, 136	0.05,+0.01	Slight dissolution.
Ta	101	0.56	Dissolution.
Fe	100	2.36	Dissolution.
Be	233	0.55	Sample pitted.
Ni	100	1.80	Dissolution.

<sup>a</sup> "+" indicates film formation resulting in weight gain of specimen.

Table VII. Chemical Compositions of Metals Tested in Molten Lithium-Sulfur Mixtures

Material	Composition, wt %					
	Fe	Ni	Cr	Mo	Mn	Other
2 RN 65 SS <sup>b</sup>	Bal <sup>a</sup>	24	17.5	4.7	1.8	0.02 C, 0.45 Si
2 RK 65 SS <sup>b</sup>	Bal	25	19.5	4.5	1.8	0.02 C, 0.45 Si, 1.5 Cu
2 RE 10 SS <sup>b</sup>	Bal	20.5	24.5	0.3	1.75	0.02 C, 0.30 Si
Worthite	Bal	24	20	3	-	2.3 Si, 1.8 Cu
347 SS	Bal	11	18	-	2	0.08 C
Carpenter 20	Bal	27	20	2.5	2	0.07 C, 1.0 Nb
Croloy 16-1	Bal	1.2	14.8	-	0.7	0.03 C
Durimet 20	45	29	20	2	-	3 Cu
Hastelloy B	5	Bal	1.0	28	-	2.5 Co
Hastelloy X	18	Bal	21	9	-	1.5 Co, 0.4 W
Inconel 600	8	76	15.5	-	0.5	
Inconel 702	1.0	Bal	1.5	-	0.5	0.05 C, 1 Si
Inconel 718	18	52.5	19	3.0	0.2	5.2 Nb, 0.8 Ti, 0.6 Al
Inconel 800	46	32.5	21	-	-	
Monel	1	64	-	-	0.8	0.2 C, 1.5 Si, 31.5 Cu
205 SS	Bal	1.3	16.6	-	15.05	0.18 C, 0.50 Si
Tenelon	Bal	0.7	18	-	16	0.1 C, 0.5 Si
LT-1	-	-	77	-	-	23 Al <sub>2</sub> O <sub>3</sub>
Zircaloy-2	0.12	-	0.1	-	-	1.5 Sn, Bal Zr

<sup>a</sup> Balance of composition.

<sup>b</sup> Product of Sandvik Steel Corporation.

Of the other materials tested, molybdenum, chromium, Zircaloy-2 and niobium were the most corrosion resistant. In a single run, molybdenum showed virtually no corrosion. Chromium was unattacked in a corrosion agitator experiment, but it was covered with a thin conductive film after an isothermal capsule test. This difference may be a result of the static conditions encountered in the capsule test as compared with the more dynamic conditions of the agitator test. Similarly, Zircaloy-2 showed little attack (0.05 mm/yr) in a corrosion agitator test but in a second experiment in a dynamic isothermal capsule experiment, low corrosion rates were observed. The sample was covered with a thin, nonconductive surface film. The reason for this difference in results between the two tests is unexplained. Niobium showed no detectable attack.

LT-1, a high-chromium cermet with  $Al_2O_3$ , was only slightly attacked in 101 hr through reduction of the  $Al_2O_3$  by lithium. This result also supports the observed good corrosion resistance of chromium. Magnesium and aluminum showed moderate corrosion rates. These materials, if usable, would significantly increase the specific energy of a lithium/sulfur battery by decreasing its weight. The variability in the magnesium and aluminum corrosion rates is attributed to differences in the protectiveness of the surface film produced by the reaction with sulfur. In some cases, the film was dense and adherent, while in others it flaked readily from the surface. The variable responsible for this difference in behavior is unknown, since all samples were exposed to what were believed to be almost identical conditions. Tantalum, iron, titanium, nickel, and beryllium showed poor corrosion resistance to lithium-sulfur mixtures.

#### b. Results of 600-Hour Tests

The screening tests of electrically conducting materials of 100 to 300 hr duration indicated the possible usefulness of several materials including Hastelloy X, Zircaloy-2, Type 205 SS, Type 347 SS, Sandvik 2 RK 65 SS, Inconel 600, and aluminum. The annual corrosion rates reported were obtained by measurement of the amount of corrosion that occurred during the 100- to 300-hr test and linear extrapolation of the measured corrosion to an annual rate. An annual rate is useful for comparing materials that have been tested for different lengths of time.

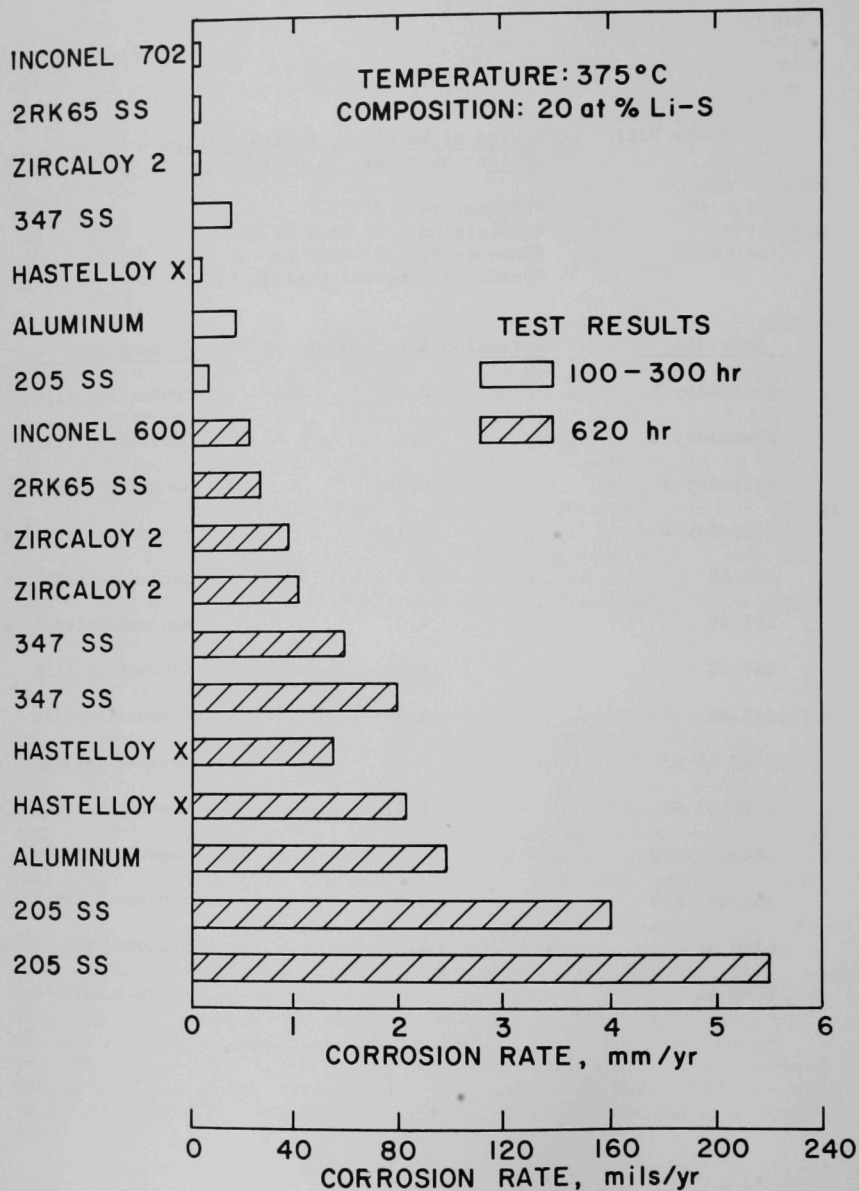
Six-hundred-hour tests were conducted to determine the effect of exposure time on the corrosion rates and to determine the validity of using linear extrapolation in obtaining annual rates. The materials tested were selected from those that had performed well in the screening tests. The tests were conducted as dynamic isothermal capsule experiments in which the candidate materials were exposed to 20 at.% lithium-sulfur mixtures at 375°C for 620 hr (about a factor of two longer than previous tests) in evacuated quartz capsules. The results of these tests are presented in Table VIII, and compared with the shorter-term tests in Figure 17.

Table VIII. Corrosion of Metals by Molten Lithium-Sulfur Mixtures: 620-hr Tests

Temperature: 375°C  
 Composition: 20 at.% Li-Se  
 Exposure Period: 620 hr  
 Dynamic Isothermal Capsule Tests

<u>Material</u>	<u>Corrosion Rate, mm/yr</u>	<u>Remarks</u>
Hastelloy X	2.0	Conductive film
Hastelloy X	1.4	Conductive film
Zircaloy-2	0.94	Nonconductive film
Zircaloy-2	1.1	Nonconductive film
205 SS	5.4	Nonconductive film
205 SS	4.0	Nonconductive film
347 SS	1.9	Conductive film
347 SS	1.5	Conductive film
2 RK 65 SS	-	Capsule failure
2 RK 65 SS	0.67	Conductive film
Inconel 600	-	Capsule failure
Inconel 600	0.54	Nonconductive film
6160 Al	2.4	Nonconductive film
6160 Al	-	Capsule failure

Figure 17. Corrosion of Metals by Molten Lithium-Sulfur Mixtures



The corrosion rates observed in the long-term tests are substantially higher than those observed in the short-term tests. This result was unexpected since most corrosion mechanisms predict a lower rate for longer-term tests. The only mechanisms which come to mind to explain these results are intergranular corrosion or a process in which a protective film (such as an oxide) is slowly reduced by lithium-sulfur mixtures and, after reduction of this film, corrosion proceeds at a rapid rate. Other possible explanations involving differences in experimental variables (such as a misplaced thermocouple causing erroneous temperature measurements) were investigated and appear to be unlikely. The three capsule failures were not surprising since quartz is not resistant to lithium-sulfur mixtures for extended periods; all failed capsules are rejected. Additional long-term tests will be made to check the validity of the data.

The results reported above indicate that while a wide variety of materials are available for cell testing for periods as long as 300 hr, the selection of materials for long-lived cells will be more restricted. All materials tested in this series showed corrosion rates lower than 0.5 mm/yr in tests of 100-300 hr duration but, if these results are correct, none would be useful in long-term cell tests. Other materials such as magnesium, chromium, molybdenum, and niobium have also shown low corrosion rates in short-term tests but have not yet been tested in long-term exposures.

Although the data obtained in these tests are useful for identifying those materials with sufficiently low corrosion rates to be of interest as cell construction materials, they should not be viewed as corrosion rates in operating cells. The data are presented in terms of mm/yr corrosion rates, calculated as the average rate observed in short-term tests. Longer-term tests may indicate lower corrosion rates since most mechanisms for corrosion have a high initial rate which decreases steadily with time. These corrosion rates were obtained in the absence of electrochemical effects which would be present in an operational cell. Such effects could significantly alter the observed corrosion rates if they enhance mass transport or affect the nature of the protective surface films produced. Therefore, these data should be used only as a guide. The actual performance of various materials should be determined by the results of long-term cell tests.

#### IV. CONCLUSIONS

The lithium/sulfur and possibly the lithium/P<sub>4</sub>S<sub>10</sub> cells should be investigated further to determine if they can be designed to achieve the performance required by electric vehicles. The voltage-current density characteristics of the cells appear to be adequate, but methods for increasing the capacity densities and sulfur utilization must be provided before these cells can be practical. Improvements in current-collector design, cell geometry, and corrosion-resistance of materials are the most appropriate areas for further work. Other variables such as cathode additives to increase electronic conductivity and decrease the viscosity of the cathode material should be investigated. The two major limitations of the cathode reaction rate appear to be the low electronic conductivity of sulfur and the slow diffusion rate of the reaction product in the cathode. It should be noted that the experiments described above were conducted with small laboratory-scale cells. No sealed cells or batteries have been tested. The construction of sealed cells suitable for a battery assembly will require a significant engineering development effort. The methods for immobilizing at least one of the three liquid phases must be improved.

Low-cost, light-weight, corrosion-resistant materials for this cell are still to be identified. The corrosion rates of potential construction materials will be investigated further.

#### ACKNOWLEDGMENTS

Messrs. F. J. Martino, P. W. Krause, J. C. Cassulo and Miss F. L. Ferry provided valuable assistance with the experimental portions of this work. Dr. A. K. Fischer is responsible for most of the work presented on filler stability. The X-ray diffraction results were provided by Mr. R. Schablaske, and Dr. M. S. Foster assisted in the conceptual design calculations for electric vehicle batteries. The advice and support of Dr. R. C. Vogel, Director of the Chemical Engineering Division, are appreciated.

## REFERENCES

1. R. S. Morse, "The Automobile and Air Pollution - A Program for Progress, Parts I and II," U. S. Department of Commerce, Dec. 1967.
2. C. D. Loeks, "Electric Vehicles and the Future City - Impact and Opportunities," Proceedings of the 1st International Electric Vehicle Symposium, Nov. 5-7, 1969, Phoenix, Ariz., p. 18, Electric Vehicle Council.
3. "Today and Tomorrow in Air Pollution," U. S. Department of Health, Education and Welfare, Public Health Service Publication No. 1555.
4. J. K. Patterson and N. Alpert, "Automotive Emission Technology," presented to the Senate Subcommittee on Air and Water Pollution, Los Angeles, Calif., February 1967.
5. E. P. Grant, California Motor Vehicle Pollution Board, Statement to the Senate Subcommittee on Air and Water Pollution, Los Angeles, Calif., February 13, 1967.
6. J. H. B. George, L. J. Stratton and R. G. Acton, "Prospects for Electric Vehicles - Electric," Arthur D. Little, Inc., report to the U. S. Department of Health, Education and Welfare, National Center for Air Pollution Control, May 15, 1968.
7. J. H. B. George, "Directions for Electric Vehicle Development," Proceedings of the 1st International Electric Vehicle Symposium, Nov. 5-9, 1969, Phoenix, Ariz., p. 29, Electric Vehicle Council.
8. K. M. Chirgwin and G. P. Kalman, "Electric Propulsion for Short-Haul Commercial Vehicles and City Buses," *Ibid.*, p. 152.
9. W. H. Shafer and T. E. Hemminger, "End-of-Run Charging for Metropolitan Area Electrically-Powered Buses," *Ibid.*, p. 339.
10. H. Shimotake, M. L. Kyle, V. A. Maroni and E. J. Cairns, "Lithium/Sulfur Cells and their Potential for Vehicle Propulsion," *Ibid.*, p. 392.
11. E. J. Cairns and H. Shimotake, "High-Temperature Batteries," *Science* 164, 1347 (1969).
12. P. R. Shipps, D. V. Ragone and A. C. Eulberg, "Advanced Secondary Battery Development for Vehicle Propulsion," Advances in Energy Conversion Engineering, *Proc. 1967 IECEC*, p. 879, ASME, New York (1967).
13. A. M. Moos and N. I. Palmer, "Zinc-Air Batteries," *Proc. 21st Ann. Power Sources Conf.*, p. 51, PSC Publications Committee, Red Bank, N. J. (1967).

14. S. M. Chodosh, E. J. Katsoulis and M. G. Rosansky, "A High Energy Density Zinc/Oxygen Battery System," *Proc. 1966 IECEC*, p. 266, AIAA, New York (1966).
15. H. N. Seiger, S. Charlip, A. E. Lyall, and R. C. Shaiz, "Organic Electrolyte Batteries," *Proc. 21st Ann. Power Sources Conf.*, p. 45, PSC Publications Committee, Red Bank, N. J. (1967).
16. D. A. J. Swinkels, "Lithium-Chlorine Battery," *J. Electrochem. Soc.* 113, p. 6 (1966).
17. T. G. Bradley, "Progress in the Development of a Rechargeable Lithium-Chlorine Electrochemical Cell," General Motors Co., Research Laboratories Report GMR-795, August, 1968.
18. R. A. Rightmire and A. L. Jones, "Fast Charge Molten Salt Batteries," *Proc. 21st Ann. Power Sources Conf.*, p. 42, PSC Publications Committee, Red Bank, N. J. (1967).
19. N. Weber and J. T. Kummer, "Sodium-Sulfur Secondary Battery," *Ibid.*, p. 37.
20. H. Shimotake and E. J. Cairns, "Bimetallic Galvanic Cells with Fused-Salt Electrolytes," *Advances in Energy Conversion Engineering*, Proc. 1967 IECEC, p. 951, ASME, New York (1967).
21. H. Shimotake, G. L. Rogers and E. J. Cairns, "Secondary Cells with Lithium Anodes and Immobilized Fused-Salt Electrolytes," *Ind. Eng. Chem. Process Des. and Dev. Quart.* 8, p. 51 (1969).
22. H. Shimotake and E. J. Cairns, "Lithium/Chalcogen Secondary Cells," *Proc. of Advances in Battery Technology Symp.*, p. 165, Southern California-Nevada Section of the Electrochem. Soc., Los Angeles, Calif., December, 1968.
23. H. Shimotake, A. K. Fischer and E. J. Cairns, "Secondary Cells with Lithium Anodes and Paste Electrolytes," *Proc. 4th IECEC*, p. 538, AIChE, New York (1969).
24. L. A. Heredy, N. P. Yao and R. C. Saunders, "Secondary Lithium-Sulfur Battery," *Proc. of the 1st International Electric Vehicle Symposium*, Nov. 5-7, 1969, Phoenix, Ariz., p. 18, Electric Vehicle Council.
25. C. E. Johnson, M. S. Foster, and M. L. Kyle, "Purification of Inert Atmospheres," *Nucl. Appl.* 3, p. 563 (1967).
26. B. Meyer, ed., Elemental Sulfur, Interscience, New York (1965).
27. H. Shimotake and E. J. Cairns, "A Lithium/Sulfur Secondary Cell with a Fused-Salt Electrolyte," Presented at the Electrochem. Soc. Meeting, New York, May, 1969, Abstr. No. 206; see also *Extended Abstracts of the Battery Div.* 5, p. 520 (1969).

28. J. R. Van Wazer, Phosphorus and Its Compounds, Interscience Publishers, Inc., New York (1958).
29. J. W. Mellor, A Comprehensive Treatise on Inorganic and Theoretical Chemistry, Vol. III, p. 663, John Wiley & Sons, Inc., New York (1961).
30. Values for the enthalpies of formation from the Handbook of Chemistry and Physics, 39th Ed., pp. 1695, 1705, Chemical Rubber Publishing Co., Cleveland (1957-1958).
31. JANAF Thermochemical Tables, Dow Chemical Co., Midland, Michigan (1960); available from the Clearinghouse for Federal Scientific and Technical Information under the number PB 168 370.
32. Chemical Engineering Division, Argonne National Laboratory, Annual Report 1969, Report ANL-7675.

X

ARGONNE NATIONAL LAB WEST



3 4444 00011572 5

